Available online at www.sciencedirect.com
SCIENCE DIRECT®
Icarus 169 (2004) 29–64
ICARUS
www.elsevier.com/locate/icarus

Surface changes on Io during the Galileo mission

Paul Geissler,[a,*] Alfred McEwen,[b] Cynthia Phillips,[c] Laszlo Keszthelyi,[a] and John Spencer[d]

[a] *U.S. Geological Survey, 2255 N. Gemini Dr., Flagstaff, AZ 86001, USA*
[b] *Lunar and Planetary Laboratory, University of Arizona, Tucson, AZ 85721, USA*
[c] *SETI Institute, 2035 Landings Drive, Mountain View, CA 94043, USA*
[d] *Lowell Observatory, 1400 W. Mars Hill Rd., Flagstaff, AZ 86001, USA*

Received 14 February 2003; revised 9 September 2003

Abstract

A careful survey of Galileo SSI global monitoring images revealed more than 80 apparent surface changes that took place on Io during the 5 year period of observation, ranging from giant plume deposits to subtle changes in the color or albedo of patera surfaces. Explosive volcanic activity was discovered at four previously unrecognized centers: an unnamed patera to the south of Karei that produced a Pele-sized red ring, a patera to the west of Zal that produced a small circular bright deposit, a large orange ring detected near the north pole of Io, and a small bright ring near Io's south pole. Only a handful of Io's many active volcanoes produced large scale explosive eruptions, and several of these erupted repeatedly, leaving at least 83% of Io's surface unaltered throughout the Galileo mission. Most of the hot spots detected from SSI, NIMS and ground-based thermal observations caused no noticeable surface changes greater than 10 km in extent over the five year period. Surface changes were found at every location where active plumes were identified, including Acala which was never seen in sunlight and was only detected through auroral emissions during eclipse. Two types of plumes are distinguished on the basis of the size and color of their deposits, confirming post-Voyager suggestions by McEwen and Soderblom [Icarus 55 (1983) 191]. Smaller plumes produce near-circular rings typically 150–200 km in radius that are white or yellow in color unless contaminated with silicates, and frequently coat their surroundings with frosts of fine-grained SO_2. The larger plumes are much less numerous, limited to a half dozen examples, and produce oval, orange or red, sulfur-rich rings with maximum radii in the north-south direction that are typically in the range from 500 to 550 km. Both types of plumes can be either episodic or quasi-continuous over a five year period. Repeated eruptions of the smaller SO_2-rich plumes likely contribute significantly to Io's resurfacing rate, whereas dust ejection is likely dominated by the tenuous giant plumes. Both types of plume deposits fade on time-scales of months to years through burial and alteration. Episodic seepages of SO_2 at Haemus Montes, Zal Montes, Dorian Montes, and the plateau to the north of Pillan Patera may have been triggered by activity at nearby volcanic centers.

Keywords: Io; Volcanism; Surfaces; Satellite

1. Introduction

Io is a major polluter of the jovian system. The small satellite trails clouds of neutral atoms that can be seen from Earth, supplies charged particles to the massive plasma torus, sheds dust than can be detected an Astronomical Unit away from Jupiter, and stains the surfaces of its neighboring satellites with a pall of yellow sulfur. Directly or indirectly, these materials derive from volcanism on Io's surface. The most dramatic signs of Io's volcanism are the energetic plumes that rise to heights of hundreds of kilometers and shower the surface with colorful pyroclastic deposits. These plumes provide a connection between geologic activity on the surface of the satellite and the flux of materials into space, both by direct ejection of dust and gas and by helping to sustain a tenuous atmosphere which is subsequently eroded by impacting charged particles. They also contribute to the rapid resurfacing that effectively disguises even the smallest impact craters on the moon's youthful surface.

At least twenty active plumes were spotted by Voyager and Galileo imaging observations (Strom et al., 1981; McEwen et al., 1998a; Keszthelyi et al., 2001). Most of these were detected during daytime observations, through the scattering of sunlight by dust particles entrained within the plumes, but certain favorably located plumes were often seen in eclipse observations through auroral emissions

* Corresponding author.
E-mail address: pgeissler@usgs.gov, geissler@lpl.arizona.edu (P. Geissler).

0019-1035/$ – see front matter
doi:10.1016/j.icarus.2003.09.024

produced by the electrically-stimulated gas molecules (Cook et al., 1981; McEwen et al., 1998a; Geissler et al., 1999a, 2001a). Because of incomplete temporal coverage, only a partial record of plume activity can be obtained through these direct sightings. A more complete history of Io's explosive eruptions must be derived by studying the surface changes that they produced.

Several questions surround the mechanisms of resurfacing, the erasure of surface deposits, the flux of materials escaping into space, and the radiation of thermal energy from Io that can only be addressed with a detailed knowledge of Io's eruption history. Galileo dust and plasma monitoring instruments detected significant variability in the concentrations of dust and charged particles from one spacecraft orbit to the next that are believed to be linked to volcanic episodes on the satellite (e.g., Krueger et al., 2002; Russell and Kivelson, 2001; Frank and Paterson, 2001), but no direct relationships have so far been established. Ground-based, NIMS and SSI observations monitored variations in thermal emission from more than 100 hot spots on Io during the Galileo era (e.g., Lopes et al., 2001) but clear links between thermal emission and eruptive style have not yet been established. It remains to be determined whether Io's thermal radiation is dominated by the eruption of new lava flows or the quiet overturning of lava lakes, a question that has significant impact on Io's resurfacing rate. It is not yet known how much of Io's prodigious resurfacing is caused by lava flows and how much is due to plume deposits, or whether the deposition of pyroclastics by plumes is dominated by the few largest plumes or the more numerous smaller plumes. Many surface changes were observed during the 4 month interval between the flybys of Voyager 1 and Voyager 2 (McEwen and Soderblom, 1983; McEwen, 1988), leading to the expectation that Io's surface might be unrecognizable by the Galileo era. Instead, only ~ 30 large-scale surface changes took place between the Voyager encounters and the start of the Galileo mission (McEwen et al., 1998a), leaving as much as 90% of the surface apparently unaltered (Geissler et al., 1999b). It is unclear whether these areas had remained inactive over the entire period or whether eruptions might have taken place but their deposits had already faded by the time of Galileo's arrival.

To begin to answer some of these questions, we have undertaken to document Io's volcanic activity during the Galileo era on the basis of surface changes seen in distant global monitoring images that were taken repeatedly throughout the 5 year mission. Section 2 describes the problems with this approach and our solutions to those problems. Section 3 presents the results of our survey, emphasizing the largest and clearest eruptions. In all, 82 candidate surface changes were found that range from giant plume deposits to subtle changes in the color or albedo of patera surfaces. We have determined as closely as possible the dates of the changes (to within the limits imposed by the imaging coverage) and attempted to distinguish between volcanic eruptions and other types of surface changes. For each volcanic plume deposit, we have made measurements of the areal extent, maximum range, and radius of any ring present. Section 4 presents analyses of these measurements, correlates surface changes with plume sightings, detections of high-temperature hot spots, and Galileo Dust Detector measurements, and discusses the relevance of the findings to the questions raised above.

2. Approach

Identification and mapping of surface changes from Galileo images is complicated by uneven temporal coverage, marked color variations that alter Io's appearance when seen through different colored filters, and photometric variations that produce dramatic contrast reversals depending upon the phase angle of the observations. Our approach was to make 3 passes through the imaging data. The first pass examined well matched color and monochrome images to identify sites of definite change and determine periods in which these areas were inactive. The second pass examined all the available images of each active volcanic center in chronological order to determine the history of its eruptions. The final step involved scrutinizing pairs of images taken before and after each identified surface change to ascertain the details of each eruption.

The greatest complication is caused by photometric effects due to varying illumination and viewing geometry; Io's surface materials vary markedly in their light scattering behavior, producing sharp color differences and contrast reversals that alter the appearance of the surface depending on whether it is illuminated obliquely or viewed with the Sun more directly behind the observer. Our approach to this problem was to compare images taken under similar photometric conditions in order to distinguish actual surface changes from photometric variations, and to identify periods in which particular volcanic centers were inactive. A computer program was developed to determine the mismatch in photometric parameters (phase angle and subsolar longitude) between each pair of monochrome images or color composites that had sufficient overlap. The results were then sorted to find the best matching pairs, and we began with these images and worked our way down the list until the photometric differences grew large enough to make actual surface changes unrecognizable. Hundreds of images were visually examined by "blinking" between pairs of pictures that were separated in time but well matched in filter, phase-angle and subsolar longitude (time of day). Each genuine surface change was identified several times by this process, in various pairs of pictures taken before and after the eruption. We have tended to be conservative in our interpretations and required that most of the surface changes showed changes in the spatial distribution of surface materials, i.e. changes in the shapes of the deposits, rather than simple changes in brightness that could be explained by photometric variations. The few sim-

ple albedo/color changes not involving changes in shape that were deemed to be due to actual surface changes (such as Camaxtli) were identified from very closely matching image pairs where photometric effects could be ruled out. These determinations were made separately for the violet, green and red/756 images because each data set contributes different information: the violet filter images best show new bright (SO_2) deposits, the green data show new red (sulfur) deposits and are often better in spatial resolution than the other global monitoring data by a factor of two, while the red/756 nm images are least susceptible to photometric variations but only show new dark (silicate) deposits. Where available, color composites made up of red/756 nm, green and violet were also compared.

The next step was to determine when each eruption took place. This involved examining time-ordered sequences of all the images that covered the volcano in question, in order to determine the date of the latest picture taken before each eruption and the earliest picture taken afterward. It is complicated by the (here unavoidable) photometric differences between consecutive images and the fact that most of the volcanic centers erupted more than once. Again, these determinations were made separately for the violet, green and red/756 image sequences; violet images were taken more frequently by Galileo than the other filters and often provided the tightest constraints on the dates of the eruptions.

As the final step in the data processing, pairs of images determined to bracket each individual surface change were analyzed in detail to determine the areas affected by each eruption, the maximum extents of the new deposits, and the radii of any rings that had appeared. Each pair of images was reprojected to an orthographic map projection centered on the origin of the disturbance (as if looking directly down on the volcanic center in question), coregistered, corrected for limb-darkening, and their brightnesses empirically matched to one another if necessary. If one of the images was taken at significantly higher resolution than the other, that image was blurred in order to simulate the appearance of the lower resolution image (however, the original unblurred images were used for the figures in Section 3). The images were then ratioed to better highlight the changed areas. Areas of new deposits were derived by hand-tracing the changes in the ratio images and include uncertainties of up to ±20%, although we attempted to be consistent in our measurement criteria. Ring radii and maximum extents were measured from either the ratio image or the youngest image of each pair, depending upon which was clearer. Ring radii were derived from diameters measured along several cords because even the smaller rings were not usually perfectly circular; the ranges listed in Section 3 represent the variability of ring radii measured in this way, rather than measurement uncertainty.

Our compiled list of surface changes during the Galileo mission is presented as Table 1. The locations of named surface features is listed using the latitudes and longitudes given in the official nomenclature list of the U.S.G.S., based on Voyager coordinates. The locations of the surface changes are derived from Galileo measurements that are often offset from the Voyager coordinates by a degree of longitude. The parameters of the images deemed to be immediately prior to and after each eruption are given in Table 2, but identifications (and the illustrations in Section 3) were frequently drawn from pairs of images that were more closely matched than those listed in Table 2. Animated sequences of consecutive Galileo images illustrating most of Io's surface changes are available at http://pirlwww.lpl.arizona.edu/~geissler/Volcanic_centers/GIF.

3. Large explosive eruptions: description and eruption history

3.1. South of Karei

3.1.1. Description

South of Karei (12° S, 13° W) is an unnamed paterae that produced a giant but faint ring late in the Galileo mission. A large, dark-floored patera adjacent to a mountain range was imaged at this location by Voyager 1. It is close to the site of an SSI hot spot seen in orbit 21 (Keszthelyi et al., 2001) and a large thermal event (designated 9906A) that was observed from Earth in June, 1996, just prior to orbit 21 (Howell et al., 2001).

3.1.2. Surface change

A Pele-sized ring appeared near the sub-Jupiter point between orbits 15 and 21 (images 449841900 to 506584100). Dark in both the green and violet filters, this faint ring (Fig. 1) was probably red in color. The deposits had largely faded by the time the area was re-imaged during orbit 22, leaving us with only a single set of green and violet filter observations upon which to base an identification. Figure 1 suggests that Io briefly had two large, oval, red rings along its equator at this time. The interior radius of the new ring was 415 ± 20 km and its exterior radius averaged 690 km (645 km in the east–west direction; 730 km N–S). The area covered by new deposits was almost 933,000 km^2. The rapid disappearance of the ring, over a period of less than two months, contrasts with the behavior of other giant rings such as those of Pele (which was continually replenished) or Tvashtar (emplaced at high northern latitudes). It is possible that these ring deposits were thin to begin with and, because of their near-equatorial location, quickly equilibrated from unstable short-chain sulfur allotropes to the yellow cyclo-octal sulfur that is common along Io's equator.

3.2. Kanehekili

3.2.1. Description

Kanehekili (18° S, 40° W) is the site of long-lived, high temperature activity that has spanned at least a decade. First noted in ground-based thermal observations in December,

Table 1
Surface changes described in this paper

	Lat	Lon	Name	Prior image	Orb	Later image	Orb	lat	lon	Area (km^2)	Range (km)	Radius (km)	Comment
1	−12	13	S. of Karei	449841900	15	506584100	21	−12	13	932700	730	690	Erupted. Giant red ring, faded by C22
2	−18	40	Kanehekili	359882742	G2	374493623	E4	−18	36	193050	290		Erupted. Lava flows, irregular deps
3	−18	40	Kanehekili	374493623	E4	383563726	E6	−18	37	207850	350	195	Erupted. Ring, diffuse deps
4	−18	40	Kanehekili	383600826	E6	401740707	C9	−19	34	78250	200		Erupted. Minor changes 6–9
5	−18	40	Kanehekili	401740707	C9	413570900	10	−19	37	69600	106		Erupted. Minor changes 9–10
6	−18	40	Kanehekili	413570900	10	420626404	11	−17	35	132250	175		Erupted. Minor changes 10–11
7	−18	40	Kanehekili	420626404	11	449841968	15	−16	36	187300	300		Erupted. Irregular diffuse dark deps
8	−69	47	Haemus Montes	374493623	E4	383600826	E6	−69	53	69700			SO_2 seepage. Brtened, same shape
9	−69	47	Haemus Montes	401740707	C9	413570900	10	−69	53	69700			SO_2 seepage. Shape of brt dep changed
10	−44	55	Masubi	401740707	C9	413570900	10	−59	54	110075	230	180	Erupted. Clear dark ring, dark spot.
11	−44	56	Masubi	449841968	15	512420523	22	−44	54	252875	215	215	Erupted. Fainter dark ring, brt deps
12	42	71	Zal Montes	383600826	E6	389654026	G7	40	81	40250			SO_2 seepage on W side of plateau
13	41	84	W. Zal	401785407	C9	413570900	10	41	84	70475	170	170	Erupted. small, brt, semicircular ring
14	41	84	W. Zal	420626404	11	506406626	21	41	84	55425	135	135	Erupted. Ring circularized, filled in
15	17	90	Gish Bar	506406626	21	520798504	24	16	89	< 1000			Patera darkened on E, C21–I24 high-res
16	17	90	Gish Bar	520798504	24	625599500	32	16	89	6000			Patera darkened on W, I24–I32 high-res
17	−16	99	Itzamna	383600826	E6	389654026	G7	−15	100	2000			Patera darkened on W side, orbits 6–7
18	80	100	N. Polar Ring	359986578	G2	374575945	E4	80	100	625000	446	446	Erupted. Brt orange, circular ring
19	26	115	Amirani	374575922	E4	383600826	E6	23	115	123125	220	200	Erupted. Dark oval ring, dark spot.
20	26	115	Amirani	383600826	E6	389654026	G7	24	116	56825	150	118	Erupted. Smaller dark ring shifted to N
21	26	115	Amirani	401785407	C9	506406118	21	20	116	70075		155	Erupted. Active plume, spokes; wht ring
22	26	115	Amirani	506406626	21	584334185	29	21	112	9950	75		Erupted. Color 21–29: dark deps to E
23	63	123	Tvashtar	506406626	21	584334185	29	63	122	1571700	780	720	Erupted. Giant red ring 275 km wide
24	40	135	Thor	584334185	29	615816245	31	39	131	278986	298	298	Erupted. Large brt ring, dark spot
25	14	136	Camaxtli	440873539	14	506406626	21	16	137	1800			Patera darkened; no ring 14–21
26	32	150	Arinna Fluctus	359986604	G2	374575922	E4	31	149	84100	200	200	Erupted. Ring shifts; wht and red deps
27	32	150	Arinna Fluctus	374575922	E4	383655107	E6	31	149	120550	200	200	Erupted. Ring darkens to W, brightened to E
28	32	150	Arinna Fluctus	440873539	14	584334178	29	31	149	64100	170	170	Erupted. Red deps to E, smaller than E4
29	−32	152	Shamash	420743485	11	440873652	14	−34	154	21925	167		Patera brightened, wht deps to S
30	−2	155	Prometheus	359986604	G2	374575922	E4	−1	155	106950	175	155	Erupted. Brt ring darkens and enlarges
31	−2	155	Prometheus	394478045	G8	401863178	C9	−1	155	21775		155	Erupted. Interior of ring changed
32	−2	155	Prometheus	401863178	C9	420773065	11	−1	155	28250	110	100	Erupted. Brt deps inside ring; dark deps N
33	−2	155	Prometheus	440873539	14	506406626	21	−1	155	65800	180	130	Erupted. Ring buried; red deps buried to E
34	−2	155	Prometheus	506406626	21	584334185	29	−1	155	125550	195	195	Erupted. Ring enlarges; red deps to E
35	−2	155	Prometheus	584334185	29	625664901	32	−1	155	65175	200	140	Erupted. Brt ring; red deps to E
36	−20	161	Culann	359986604	G2	374575922	E4	−20	161	131150	210	165	Erupted. New deps to S, E; ring to N, W
37	−20	161	Culann	374575922	E4	383655107	E6	−20	161	123825	220		Erupted. Brt deps to N, SE, W; ring to NE
38	−20	161	Culann	401863178	C9	420773065	11	−20	161	7175	130		Erupted. Brt deps to S at W edge of red deps
39	−20	161	Culann	440873539	14	506406626	21	−20	161	7075	75		Erupted. Red deps to N, close to source
40	−20	161	Culann	506406626	21	584334185	29	−20	161	23375	175		Erupted. Minor changes 21–29: see color
41	−70	170	S. Polar Ring	440873652	14	506406118	21	−70	170	190100	245	237	Erupted. Brt ring in Illyrikon Regio
42	18	173	Zamama	359986604	G2	374575922	E4	18	171	135775	250	185	Erupted. Irregular brt ring; dark deps to N, W
43	18	173	Zamama	374575922	E4	383655107	E6	19	175	37275	170		Erupted. Flows broadened; brt deps at margins
44	18	173	Zamama	394478123	G8	401863204	C9	18	172	62000		140	Erupted. Faint ring; area from radius
45	18	173	Zamama	401863204	C9	440873652	14	19	175	95800		150	Erupted. Red deps to W; enlarged brt ring
46	18	173	Zamama	440873652	14	506406118	21	19	172	65300	170		Erupted. Red, wht deps to W
47	18	173	Zamama	506406118	21	584334178	29	8	172	61575		140	Erupted. Brt ring especially to N
48	18	173	Zamama	584334185	29	625664901	32	18	176	13500	85		Erupted. Possible refreshed red deps to W
49	−30	204	Dorian Montes	584334185	29	625664901	32	−30	204	15325			SO_2 seepage.
50	−32	206	Marduk	359986604	G2	383655107	E6	−24	211	177325	270	250	Erupted. Deps W, S of flows, around flows
51	−32	206	Marduk	383655107	E6	506492200	21	−23	211	132175	210	210	Erupted. Ring darkened, shifted; brt deps
52	−32	206	Marduk	506492200	21	520873426	24	−25	212	149375	250	208	Erupted. Yellow ring; changed brt and red deps
53	−32	206	Marduk	520873426	24	584334178	29	−22	208	12525	130		Erupted. Brt deps to NE; refreshed ring
54	−32	206	Marduk	584334185	29	625664901	32	−27	211	28675	115		Erupted. Sulfur lava flow seen 506–625

(*continued on next page*)

Table 1 (*Continued*)

	Lat	Lon	Name	Prior image	Orb	Later image	Orb	lat	lon	Area (km^2)	Range (km)	Radius (km)	Comment
55	−9	234	Kaminari	394519123	G8	413744204	10	−8	234	1775			Erupted. Wht deps from under Pillan ash
56	−9	234	Kaminari	420832945	11	506501100	21	−9.7	233	47725		92	Erupted. Wht ring 10–21; happened after E11
57	−9	234	Kaminari	506492200	21	520873452	24	−8	237	14525	150		Erupted. Irregular brt deps to W, N
58	−13	234	Reiden	394519123	G8	413744204	10	−13	236	10275			Erupted. Active during Pillan eruption
59	−13	234	Reiden	413744204	10	506492200	21	−13	236	6325		45	Erupted. Small wht ring
60	−13	234	Reiden	413744179	10	520873426	24	−13	235	2750	60		Erupted. Red deps to E of Reiden
61	−12	242	Pillan	349673952	G1	359986578	G2	−12	243	2100			Patera darkened G1–G2 color
62	−12	242	Pillan	359986578	G2	383758500	E6	−12	243	2100			Patera brightened G2–E6 color
63	−12	242	Pillan	383758500	E6	394552445	G8	−12	243	2100			Patera brightened E6–G8 color
64	−12	242	Pillan	394519123	G8	413744204	10	−11	242	205400	254	244	Erupted. Centered on lava flows E of caldera
65	−12	242	Pillan	420832945	11	506492200	21	−12	243	2100			Patera darkened 11–21
66	−18	256	Pele	349673952	G1	383758500	E6	−18	255	1014450	650	540	Erupted. Ring expands, covers wht dep to W
67	−18	256	Pele	389772007	G7	394552545	G8	−18	255	515600	425		Erupted. Minor changes in ring G7–G8.
68	−18	256	Pele	394552445	G8	413744179	10	−18	255	625850	530		Erupted. Ring changes; new deps W, S
69	−18	256	Pele	413744204	10	420833023	11	−18	255	894000	545		Erupted. Enlarged to W; darkens to E, S
70	−18	256	Pele	420833023	11	506484107	21	−18	255	697075	580		Erupted. Ring changes shape
71	−18	256	Pele	506501107	21	520873452	24	−18	255	1009225	720		Erupted. Obvious changes to ring
72	−18	256	Pele	520873426	24	584396885	29	−18	255	615975	530		Erupted. Buries Pillan; wht mtls in red ring
73	−18	256	Pele	584396885	29	625700552	32	−18	255	671350	580		Erupted. Minor ring changes
74	54	300	Dazhbog	389772000	G7	520873426	24	55	300	6600			Patera darkened, perhaps by 506501100
75	54	300	Dazhbog	584396885	29	615693245	31	55	300	581900	480	425	Erupted. Orange oval ring; interior brt ring
76	38	307	Amaterasu	349746326	G1	383758507	E6	38	306	4500			Patera darkened G1–E6
77	−6	311	N. of Mazda	383758500	E6	413791545	10	−6	311	2000			Patera brightened; dark spot turns wht
78	−6	311	N. of Mazda	413791545	10	450110900	15	−6	311	2000			Patera darkened; wht spot turns black
79	−9	325	Ra	349746326	G1	383758507	E6	−10	323	170050	260		Erupted. Yellow deps to N in G1–E6
80	11	333	Acala Fluctus	383758500	E6	420626378	11	10	335	141975	260		Erupted. Dark spot; brt deps to W, S, and E
81	11	333	Acala Fluctus	450110968	15	506572423	21	12	331	149775	250	140	Erupted. Quasicircular brt deps E of fluctus
82	46	338	Surt	512336700	22	615693245	31	42	335	470875	390	390	Erupted. Suspected orange ring; red deps

Lat: latitude of named feature; Lon: west longitude of named feature; prior image: last observation before surface change; orb: orbit number; later image: first observation after surface change. lat: latitude of center of changed area; lon: longitude of center of changed area; area: area of surface change; range: maximum extent of plume deposit, if present; radius: radius of ring, if present.

Table 2
Image parameters

	Prior image	Filter	Phase (deg)	Res. (km)	Year:day:time	Orbit and picture	Later image	Filter	Phase (deg)	Res. (km)	Year:day:time	Orbit and picture
1	449841900	COLOR	76.5	14.2	1998:150:23:57	15I0001	506584100	GREEN	69.54	16.8	1999:184:10:04	21I0335
2	359882742	VIOLET	24.34	16	1996:250:08:11	G2I0068	374493623	VIOLET	33.54	15.9	1996:352:22:23	E4I0013
3	374493623	VIOLET	33.54	15.9	1996:352:22:23	E4I0013	383563726	VIOLET	46.01	15.7	1997:050:14:52	E6I0022
4	383600826	VIOLET	30.56	10.9	1997:050:21:07	E6I0032	401740707	VIOLET	4.49	21	1997:178:06:01	C9I0007
5	401740707	VIOLET	4.49	21	1997:178:06:01	C9I0007	413570900	VIOLET	36.04	10.6	1997:261:07:37	10I0012
6	413570900	VIOLET	36.04	10.6	1997:261:07:37	10I0012	420626404	VIOLET	0.61	20.8	1997:310:20:36	11I0007
7	420626404	VIOLET	0.61	20.8	1997:310:20:36	11I0007	449841968	VIOLET	76.45	14.2	1998:150:23:58	15I0003
8	374493623	VIOLET	33.54	15.9	1996:352:22:23	E4I0013	383600826	VIOLET	30.56	10.9	1997:050:21:07	E6I0032
9	401740707	VIOLET	4.49	21	1997:178:06:01	C9I0007	413570900	VIOLET	36.04	10.6	1997:261:07:37	10I0012
10	401740707	VIOLET	4.49	21	1997:178:06:01	C9I0007	413570900	VIOLET	36.04	10.6	1997:261:07:37	10I0012
11	449841968	VIOLET	76.45	14.2	1998:150:23:58	15I0003	512420523	VIOLET	72.21	15.9	1999:225:09:37	22I0010
12	383600826	VIOLET	30.56	10.9	1997:050:21:07	E6I0032	389654026	VIOLET	41.59	10.5	1997:093:09:11	G7I0022
13	401785407	VIOLET	47.01	16.6	1997:178:13:33	C9I0013	413570900	VIOLET	36.04	10.6	1997:261:07:37	10I0012
14	420626404	VIOLET	0.61	20.8	1997:310:20:36	11I0007	506406626	COLOR M	3.95	1.29	1999:183:04:09	21I0155
15	506406626	COLOR M	3.95	1.29	1999:183:04:09	21I0155	520798504	CLEAR	20.1	0.25	1999:284:05:27	24I0117
16	520798504	CLEAR	20.1	0.25	1999:284:05:27	24I0117	625599500	CLEAR	46.79	0.25	2001:289:02:21	32I0028
17	383600826	VIOLET	30.56	10.9	1997:050:21:07	E6I0032	389654026	VIOLET	41.59	10.5	1997:093:09:11	G7I0022
18	359986578	COLOR	4.1	4.93	1996:251:01:41	G2I0073	374575945	COLOR	0.48	5.87	1996:353:12:15	E4I0019
19	374575922	VIOLET	0.48	11.8	1996:353:12:15	E4I0018	383600826	VIOLET	30.56	10.9	1997:050:21:07	E6I0032
20	383600826	VIOLET	30.56	10.9	1997:050:21:07	E6I0032	389654026	VIOLET	41.59	10.5	1997:093:09:11	G7I0022
21	401785407	VIOLET	47.01	16.6	1997:178:13:33	C9I0013	506406118	VIOLET	3.95	1.29	1999:183:04:09	21I0155
22	506406626	COLOR M	3.95	1.29	1999:183:04:09	21I0155	584334185	COLOR	21.93	10.3	2000:365:08:23	29I0011
23	506406626	COLOR M	3.95	1.29	1999:183:04:09	21I0155	584334185	COLOR	21.93	10.3	2000:365:08:23	29I0011

(*continued on next page*)

Table 2 (*Continued*)

	Prior image	Filter	Phase (deg)	Res. (km)	Year:day:time	Orbit and picture	Later image	Filter	Phase (deg)	Res. (km)	Year:day:time	Orbit and picture
24	584334185	COLOR	21.93	10.3	2000:365:08:23	29I0011	615816245	COLOR	27.4	19.9	2001:220:09:42	31I0063
25	440873539	COLOR M	35.99	2.99	1998:088:00:37	14I0001	506406626	COLOR M	3.95	1.29	1999:183:04:09	21I0155
26	359986604	VIOLET	4.1	9.85	1996:251:01:41	G2I0075	374575922	VIOLET	0.48	11.8	1996:353:12:15	E4I0018
27	374575922	VIOLET	0.48	11.8	1996:353:12:15	E4I0018	383655107	VIOLET	23.57	10.2	1997:051:06:16	E6I0042
28	440873539	COLOR M	35.99	2.99	1998:088:00:37	14I0001	584334178	VIOLET	21.94	10.3	2000:365:08:23	29I0010
29	420743485	VIOLET	108.1	8.98	1997:311:16:20	11I0015	440873652	VIOLET	35.99	2.99	1998:088:00:37	14I0001
30	359986604	VIOLET	4.1	9.85	1996:251:01:41	G2I0075	374575922	VIOLET	0.48	11.8	1996:353:12:15	E4I0018
31	394478045	COLOR	80.8	9.77	1997:127:06:08	G8I0007	401863178	COLOR	80.89	6.15	1997:179:02:40	C9I0015
32	401863178	COLOR	80.89	6.15	1997:179:02:40	C9I0015	420773065	COLOR	113.5	8.2	1997:311:21:19	11I0016
33	440873539	COLOR M	35.99	2.99	1998:088:00:37	14I0001	506406626	COLOR M	3.95	1.29	1999:183:04:09	21I0155
34	506406626	COLOR M	3.95	1.29	1999:183:04:09	21I0155	584334185	COLOR	21.93	10.3	2000:365:08:23	29I0011
35	584334185	COLOR	21.93	10.3	2000:365:08:23	29I0011	625664901	COLOR	48.82	5.06	2001:289:13:22	32I0043
36	359986604	VIOLET	4.1	9.85	1996:251:01:41	G2I0075	374575922	VIOLET	0.48	11.8	1996:353:12:15	E4I0018
37	374575922	VIOLET	0.48	11.8	1996:353:12:15	E4I0018	383655107	VIOLET	23.57	10.2	1997:051:06:16	E6I0042
38	401863178	COLOR	80.89	6.15	1997:179:02:40	C9I0015	420773065	COLOR	113.5	8.2	1997:311:21:19	11I0016
39	440873539	COLOR M	35.99	2.99	1998:088:00:37	14I0001	506406626	COLOR M	3.95	1.29	1999:183:04:09	21I0155
40	506406626	COLOR M	3.95	1.29	1999:183:04:09	21I0155	584334185	COLOR	21.93	10.3	2000:365:08:23	29I0011
41	440873652	VIOLET	35.99	2.99	1998:088:00:37	14I0001	506406118	VIOLET	3.95	1.29	1999:183:04:09	21I0155
42	359986604	VIOLET	4.1	9.85	1996:251:01:41	G2I0075	374575922	VIOLET	0.48	11.8	1996:353:12:15	E4I0018
43	374575922	VIOLET	0.48	11.8	1996:353:12:15	E4I0018	383655107	VIOLET	23.57	10.2	1997:051:06:16	E6I0042
44	394478123	VIOLET	80.83	9.76	1997:127:06:09	G8I0009	401863204	VIOLET	80.89	12.3	1997:179:02:40	C9I0017
45	401863204	VIOLET	80.89	12.3	1997:179:02:40	C9I0017	440873652	VIOLET	35.99	2.99	1998:088:00:37	14I0001
46	440873652	VIOLET	35.99	2.99	1998:088:00:37	14I0001	506406118	VIOLET	3.95	1.29	1999:183:04:09	21I0155
47	506406118	VIOLET	3.95	1.29	1999:183:04:09	21I0155	584334178	VIOLET	21.94	10.3	2000:365:08:23	29I0010
48	584334185	COLOR	21.93	10.3	2000:365:08:23	29I0011	625664901	COLOR	48.82	5.06	2001:289:13:22	32I0043
49	584334185	COLOR	21.93	10.3	2000:365:08:23	29I0011	625664901	COLOR	48.82	5.06	2001:289:13:22	32I0043
50	359986604	VIOLET	4.1	9.85	1996:251:01:41	G2I0075	383655107	VIOLET	23.57	10.2	1997:051:06:16	E6I0042
51	383655107	VIOLET	23.57	10.2	1997:051:06:16	E6I0042	506492200	VIOLET	29.39	9.96	1999:183:18:34	21I0285
52	506492200	VIOLET	29.39	9.96	1999:183:18:34	21I0285	520873426	COLOR	31.36	6.68	1999:284:18:05	24I0145
53	520873426	COLOR	31.36	6.68	1999:284:18:05	24I0145	584334178	VIOLET	21.94	10.3	2000:365:08:23	29I0010
54	584334185	COLOR	21.93	10.3	2000:365:08:23	29I0011	625664901	COLOR	48.82	5.06	2001:289:13:22	32I0043
55	394519123	VIOLET	85.24	10.5	1997:127:13:03	G8I0018	413744204	VIOLET	60.96	10.3	1997:262:12:50	10I0028
56	420832945	COLOR	99.29	10.5	1997:312:07:25	11I0022	506501100	GREEN	32.22	11.9	1999:183:20:04	21I0290
57	506492200	VIOLET	29.39	9.96	1999:183:18:34	21I0285	520873452	VIOLET	31.37	6.69	1999:284:18:05	24I0147
58	394519123	VIOLET	85.24	10.5	1997:127:13:03	G8I0018	413744204	VIOLET	60.96	10.3	1997:262:12:50	10I0028
59	413744204	VIOLET	60.96	10.3	1997:262:12:50	10I0028	506492200	VIOLET	29.39	9.96	1999:183:18:34	21I0285
60	413744179	COLOR	60.97	5.14	1997:262:12:50	10I0025	520873426	COLOR	31.36	6.68	1999:284:18:05	24I0145
61	349673952	COLOR	54.61	13.9	1996:178:15:49	G1I0005	359986578	COLOR	4.1	4.93	1996:251:01:41	G2I0073
62	359986578	COLOR	4.1	4.93	1996:251:01:41	G2I0073	383758500	COLOR	13.91	5.62	1997:051:23:41	E6I0060
63	383758500	COLOR	13.91	5.62	1997:051:23:41	E6I0060	394552445	COLOR	73.67	11.4	1997:127:18:40	G8I0019
64	394519123	VIOLET	85.24	10.5	1997:127:13:03	G8I0018	413744204	VIOLET	60.96	10.3	1997:262:12:50	10I0028
65	420832945	COLOR	99.29	10.5	1997:312:07:25	11I0022	506492200	VIOLET	29.39	9.96	1999:183:18:34	21I0285
66	349673952	COLOR	54.61	13.9	1996:178:15:49	G1I0005	383758500	COLOR	13.91	5.62	1997:051:23:41	E6I0060
67	389772007	VIOLET	36.79	12.2	1997:094:05:04	G7I0052	394552545	VIOLET	73.61	11.4	1997:127:18:41	G8I0021
68	394552445	COLOR	73.67	11.4	1997:127:18:40	G8I0019	413744179	COLOR	60.97	5.14	1997:262:12:50	10I0025
69	413744204	VIOLET	60.96	10.3	1997:262:12:50	10I0028	420833023	VIOLET	99.28	10.5	1997:312:07:26	11I0024
70	420833023	VIOLET	99.28	10.5	1997:312:07:26	11I0024	506484107	VIOLET	27.56	8.39	1999:183:17:13	21I0282
71	506501107	VIOLET	32.21	11.9	1999:183:20:05	21I0292	520873452	VIOLET	31.37	6.69	1999:284:18:05	24I0147
72	520873426	COLOR	31.36	6.68	1999:284:18:05	24I0145	584396885	COLOR	14.39	17.3	2000:365:18:57	29I0015
73	584396885	COLOR	14.39	17.3	2000:365:18:57	29I0015	625700552	COLOR	36.9	9.94	2001:289:19:23	32I0050
74	389772000	GREEN	36.8	12.2	1997:094:05:04	G7I0050	520873426	COLOR	31.36	6.68	1999:284:18:05	24I0145
75	584396885	COLOR	14.39	17.3	2000:365:18:57	29I0015	615693245	COLOR	3.55	19.6	2001:219:12:58	31I0060
76	349746326	VIOLET	25.3	15.3	1996:179:04:01	G1I0012	383758507	VIOLET	13.92	11.2	1997:051:23:41	E6I0062
77	383758500	COLOR	13.91	5.62	1997:051:23:41	E6I0060	413791545	COLOR	74.56	10.5	1997:262:20:49	10I0038
78	413791545	COLOR	74.56	10.5	1997:262:20:49	10I0038	450110900	COLOR	65.47	12.5	1998:152:21:17	15I0060
79	349746326	VIOLET	25.3	15.3	1996:179:04:01	G1I0012	383758507	VIOLET	13.92	11.2	1997:051:23:41	E6I0062
80	383758500	COLOR	13.91	5.62	1997:051:23:41	E6I0060	420626378	COLOR	0.61	10.4	1997:310:20:36	11I0005
81	450110968	VIOLET	65.54	12.6	1998:152:21:18	15I0062	506572423	VIOLET	63.99	15.3	1999:184:08:06	21I0331
82	512336700	GREEN	4.02	9.55	1999:224:19:29	22I0004	615693245	COLOR	3.55	19.6	2001:219:12:58	31I0060

Characteristics of the image pairs bracketing the surface changes listed in Table 1. Prior image: last observation before surface change; filter: filter name; "COLOR" is listed when the image is part of a set of 3 or more colors, and "COLORM" when the image is part of a color mosaic; phase: phase angle; res: image resolution per pixel; orbit and picture: Galileo picture number (the first 2 digits give the orbit number); later image: first observation after surface change.

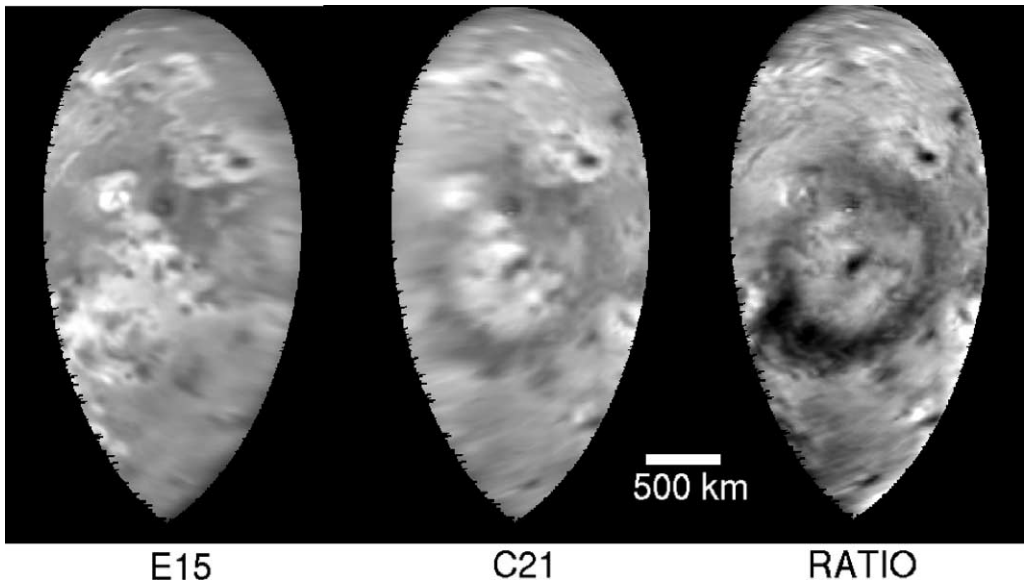

Fig. 1. Surface changes south of Karei: green filter images. Shortly before orbit C21, a giant plume from an unnamed patera emplaced a faint ring that measured 1400 km in diameter.

1989 (Spencer et al., 1990), variable thermal emission was recorded from this location until May, 1993 (Spencer and Schneider, 1996) and was detected again in 1996, just prior to the first Galileo observations (Spencer et al., 1997a). It is also the possible site of an earlier thermal outburst (defined as a doubling of the 5 μ flux) that was recorded in 1986 (Goguen et al., 1988; Veeder et al., 1994). Kanehekili may have been active during the Voyager flybys, but the IRIS instruments did not detect thermal emission from the region in 1979 (perhaps because of unfavorable observing conditions) and no plume was observed. HST observations (Spencer et al., 1997b) showed that the appearance of the region had altered between the Voyager flybys and 1994.

High temperature thermal emission from Kanehekili was observed repeatedly by both Galileo NIMS and SSI. Beginning in orbit 4, SSI eclipse observations resolved two separate hot spots spaced approximately 100 km apart, perhaps arising from lava exposed at the source vent and at the toe of a lava flow (McEwen et al., 1998a). The best resolution (Voyager 1) image of the region shows low-albedo materials in the area that are made up of extensive lava flows and dark pyroclastic deposits. Subsequent SSI eclipse observations detected high-temperature (> 1000 K) hot spots on orbits 7, 8, 10, 11, and 15 (McEwen et al., 1998a; Keszthelyi et al., 2001). NIMS also observed Kanehekili numerous times during the Galileo mission, starting in orbit 4 (Lopes-Gautier et al., 1999). Sunlit plumes were sighted over Kanehekili on orbits 8 and 11, and auroral glows were seen in the region during orbits 11, 14, and 21.

3.2.2. Surface changes

Kanehekili produced at least three major eruptions (Fig. 2) and several minor surface changes that were observed by Galileo SSI, all centered on the southernmost of the two hot spots. A detailed description of the largest of these surface changes is provided by Phillips (2000). The area was imaged on 10 separate occasions, on orbits 1, 2, 4, 6, 9, 10, 11, 15, 22, and 31. No discernable activity can be seen in the earliest low quality images from orbits 1 and 2, but a major change occurred between orbits 2 and 4 (images 359882742 and 374493623) that was earmarked by extensive bright and dark pyroclastic deposits and a change in the shape of the central low albedo materials from roughly rectangular to pear-shaped. New bright materials were deposited to the west and south of Kanehekili in an irregular pattern, reaching a maximum range of 290 km from the center of the disturbance. The area covered by new bright and dark deposits was $\sim 193{,}000$ km^2. A second major eruption followed immediately, during the interval between orbits 4 and 6 (images 374493623 and 383563726). This eruption produced a clearly defined ring, 195 km in radius, that was centered on 18S37. Surrounding the ring were emplaced irregular diffuse deposits of bright materials to the east and dark materials to the north and northwest, out to a maximum distance of 250 to 350 km from the ring center. Our best estimate of the area affected is 208,000 km^2, of which $\sim 120{,}000$ km^2 were interior to the ring. Less dramatic, but still noticeable changes ensued in the intervals between orbits 6 and 9, orbits 9 and 10, and orbits 10 and 11, during which the ring faded and was replaced by a bright band that formed along the margin of the central dark deposit (presumably lava flows). This bright band was overcoated by dark materials in the last major eruption, between orbits 11 and 15 (images 420626404 to 449841968). This eruption emplaced diffuse dark deposits in an irregular pattern out to a range of ~ 300 km and affected an area of 187,000 km^2. By the time Kanehekili was imaged again, in orbit 22, the central dark feature had darkened and was again surrounded by bright materials except in the north. Subsequent coverage

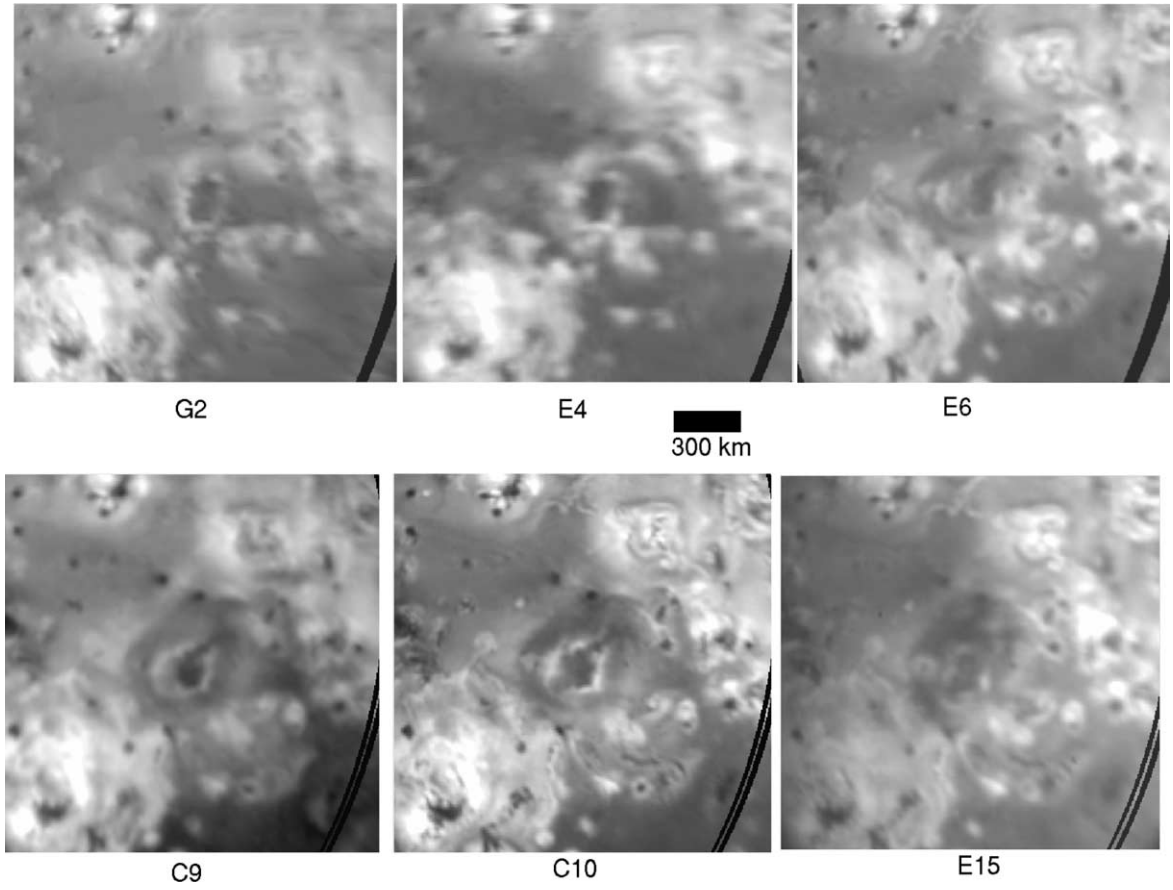

Fig. 2. Surface changes at Kanehekili: violet filter images. Sustained activity at this volcano was indicated by frequent changes in both the central dark deposits and the bright rim around them.

(orbit 31 only) was at a resolution insufficient to determine whether Kanehekili's activity continued.

3.3. Masubi/Haemus Montes

3.3.1. Description

Masubi (44° S, 55° W) was the source of prominent plumes observed by both Voyager 1 and Voyager 2 (Strom and Schneider, 1982), although the Voyager IRIS instruments failed to detect thermal emission from the region. The region had brightened beyond its Voyager appearance by 1993 (Sartoretti et al., 1995) and further changes were apparent in HST imaging acquired in 1994 (Spencer et al., 1997b). A broad ring surrounded the volcanic center in Voyager 2 images but was absent by the time of the first Galileo observations (Phillips, 2000). No high-resolution images of Masubi were acquired by either of the Voyagers or by Galileo, but the volcanic center appears to be a low-albedo spot near the middle of a large, dark linear feature known as Masubi Fluctus. To the south of Masubi lies Haemus Mons, a ~ 10 km high mountain that is surrounded by a bright halo of SO_2. NIMS detected thermal emission near 53° $\pm$ 12° S, 52° $\pm$ 12° W during orbit 11 that was attributed to Masubi (Lopes et al., 2001), but no high-temperature hot spot has been detected by SSI. Ground-based observations (Goguen and Davies, 1999) recorded high temperature thermal emission on August 21, 1998, between orbits 16 and 17. Plumes were seen in sunlit images during orbits 21 and 22 (Keszthelyi et al., 2001) and faint, diffuse glows were seen from the region in several early eclipse images (McEwen et al., 1998a). Later activity was detected by NIMS and ground-based observations from orbits 31 onward (Lopes et al., 2003; de Pater et al., 2004). The Masubi region was characterized by unusually forward-scattering photometric properties, interpreted by Geissler et al. (2001b) to be caused by frosts of fine-grained SO_2 that may indicate recent volcanic activity.

3.3.2. Surface changes

A detailed description of Masubi's surface changes is given by Phillips (2000). The area was imaged on 9 separate occasions, on orbits 1, 2, 4, 6, 9, 10, 11, 15, and 22. Two distinct eruptions were observed by Galileo that produced prominent rings around Masubi (Fig. 3). The first occurred between orbits 9 and 10 (images 401740707 to 413570900) and left a prominent dark ring 180 ± 10 km in radius, surrounded by a fainter bright ring up to 230 km in radius. A new dark spot formed at the center of these rings, located at 59° S, 54° W. The total area covered by the dark and bright rings and the new dark spot was ap-

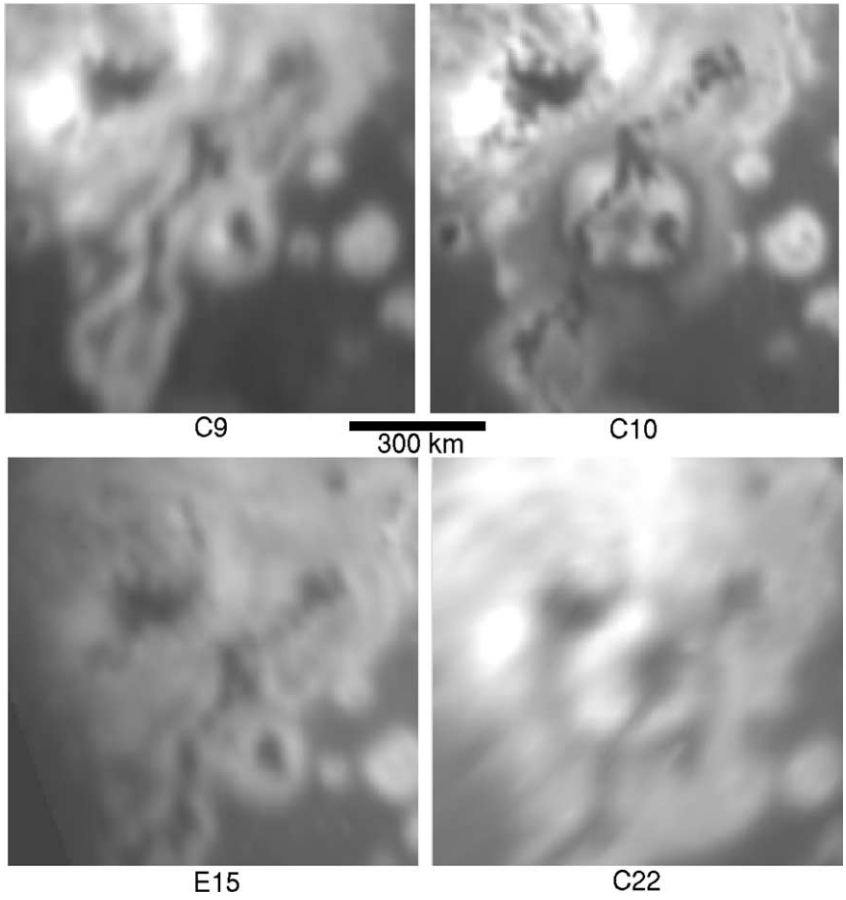

Fig. 3. Surface changes at Masubi: violet filter images. Two distinct rings emplaced by orbits C10 and C22 had different sizes and center locations.

proximately 110,000 km^2. The rings began to fade by the time of the next observation (orbit 11) and had completely disappeared by orbit 15, 8 months after their emplacement. The second eruption occurred between orbits 15 and 22 (images 449841968 and 512420523), perhaps associated with the high-temperature thermal emission seen by Goguen and Davies in August, 1998. It deposited a fainter dark ring centered on 44° S, 54° W, approximately 125 km to the north of the earlier eruption. The new ring was larger (215 ± 10 km) and the interior of the ring was coated with new bright materials. New bright materials were also emplaced to the south of Masubi, possibly in a separate eruption. The total area affected (everything inside the ring plus the southern bright materials) totaled 251,000 km^2. Subsequent coverage was inadequate to distinguish further changes after orbit 22.

In addition to these volcanic eruptions, Phillips (2000) describes a brightening of the bright halo surrounding Haemus Mons between Voyager 2 and Galileo orbit 1, that she attributes to possible episodic seepage (sapping) of SO_2 from the base of the massif. We note that a second such brightening may have occurred between orbits 9 and 10 (images 401740707 to 413570900), affecting an area of $\sim$ 70,000 km^2. Such interpretations are made difficult by the sloping terrain associated with the local topography.

3.4. West of Zal/Zal Montes

3.4.1. Description

West Zal (41° N, 84° W) is an unnamed patera to the west of Zal Montes. It lies outside the error limits for the location of the NIMS hot spot designated "Zal." To our knowledge it has not been previously mentioned in the literature.

Zal (42° N, 76° W) is a large patera bounded on its western side by a fault scarp and a broad plateau that rises 1.4–1.9 km above the surrounding plains (Turtle et al., 2001). Dark lava flows appear to have erupted from the base of the fault scarp and flowed eastwards across the patera floor (Radebaugh et al., 2001). Bright red deposits are found farther south along the fault scarp, which terminates in a small dark patera at 34° N, 73° W. High-temperature thermal emission was spotted by SSI along the fault scarp south of Zal (36°–37° N, 76° W) during orbits 7, 8, and 15 (McEwen et al., 1998a; Keszthelyi et al., 2001), whereas NIMS observed emission likely located at the main patera ($37° \pm 3°$ N, $78° \pm 3°$ W) (Lopes et al., 2003).

Zal Montes is the 60 km by 150 km plateau that lies between West Zal and Zal paterae. Its western slopes are characterized by hummocks and scallops (alcoves) that are interpreted by Moore et al. (2001) to be caused by sapping of SO_2.

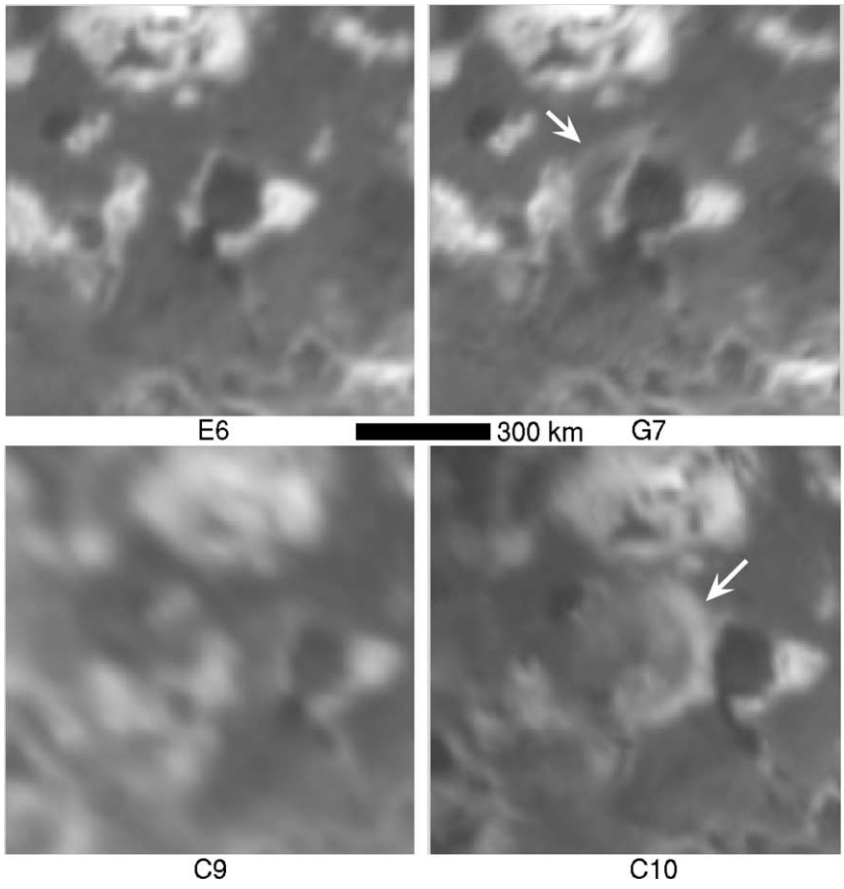

Fig. 4. Surface changes in the Zal area: violet filter images. Two different types of surface changes are interpreted in the area west of Zal. First, a brightening occurred along the base of the Zal Montes plateau between orbits E6 and G7 that may have been caused by seepage of SO_2. Later, between orbits C9 and C10, a bright semicircular ring was emplaced around an unnamed patera that continued to erupt until some time before orbit C21 (see color Plate 1, part A).

3.4.2. Surface changes

This region was observed by SSI on 13 separate occasions, on orbits 1, 2, 6, 7, 8, 9, 10, 11, 21, 22, 25, 27, and 31. The first sign of activity was the appearance of a single bright ring along the western slopes of Zal Montes plateau between orbits 6 and 7 (images 383600826 to 389654026; Fig. 4). The deposit persisted through the next observation on orbit 8 but had largely faded by orbit 9, no more than 6 months after it was emplaced. Because it appeared on the western side of Zal Montes plateau, opposite to Zal Patera, and did not continue on the eastern side of the plateau (closer to Zal Patera), we suggest that this deposit was not produced by a volcanic plume but instead formed by episodic seepage of SO_2 from the base of the plateau in a manner similar to that suggested by Phillips (2000) for Haemus Mons. It is possible that the episode was triggered by volcanic activity along the fault scarp that separates the patera from the plateau; the event occurred just prior to the SSI observation of high temperature lava in this area, and changes are also seen near Zal Patera (a brightening of the patera floor and an obscuration of the bright deposits to the south of Zal).

Between orbits 9 and 10 (images 401785407 and 413570900) the unnamed patera West of Zal erupted and overprinted the existing bright deposits with a small bright ring with a radius of 170 km, particularly noticeable toward the east. Radial "spokes" in the latter image suggest that the plume may have been active at the time it was imaged during orbit 10. The semicircular area affected by the eruption totaled only 70,000 km^2. It is possible that this eruption was responsible for the dark streaks that were later seen draped across the western scarp of Zal Montes in orbits 25 and 27. The asymmetric appearance of the plume deposit (brighter toward the east) persisted through orbit 11, but the deposit had circularized and contracted to a radius of 135 km by orbit 21 and the interior had been filled in so that the deposits then covered a total area of $\sim$ 55,000 km^2. Plate 1A compares the appearance of this region in well-matched color images from orbits 4 and 21. No spokes are seen in the orbit 21 image, and the deposit appears whitish rather than the characteristic blue of active plumes, so it is likely that the eruption was inactive by the time of the orbit 21 observations. No further activity was seen in the later high-resolution limb images of nearby Zal during orbits 25 and 27.

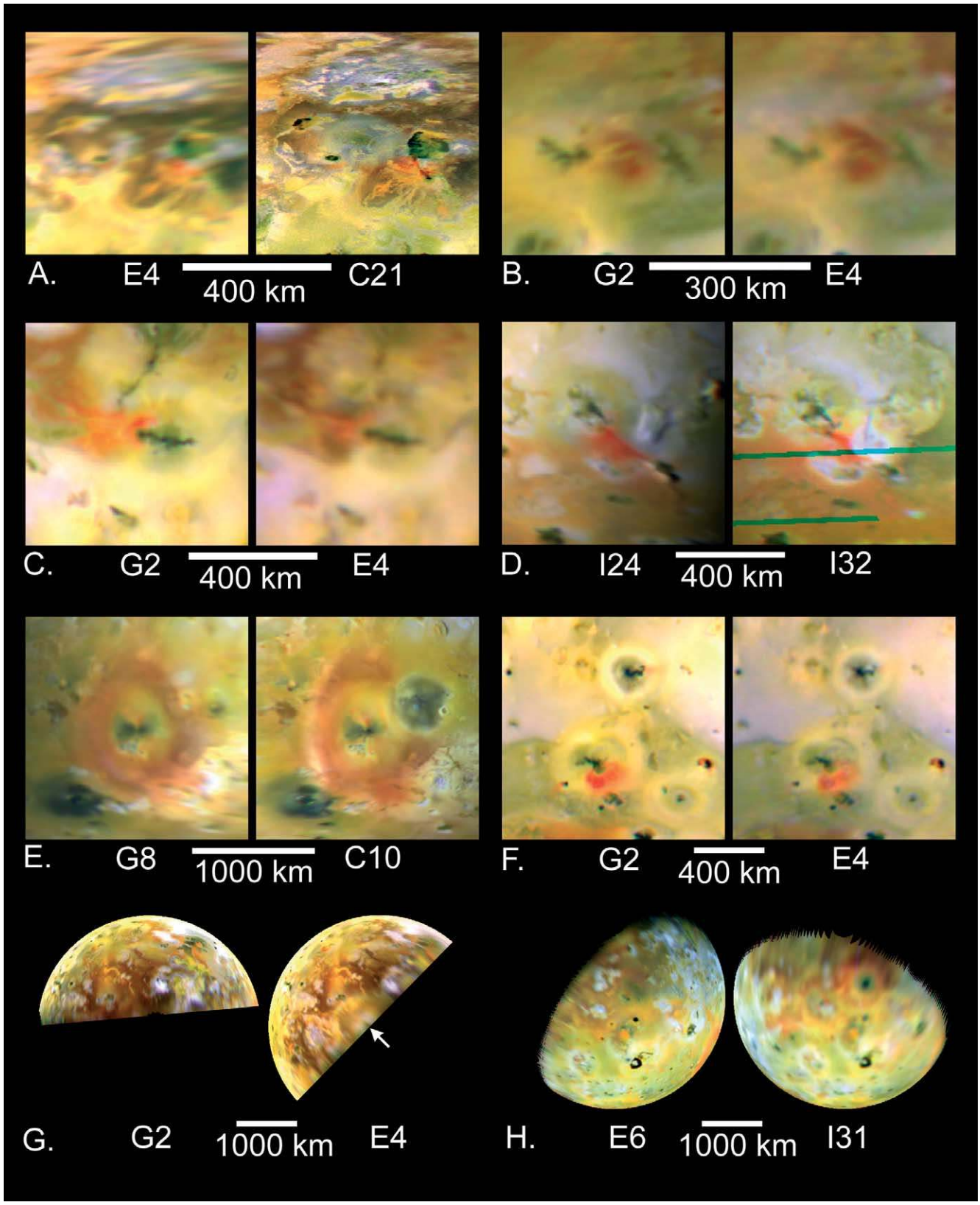

Plate 1. Montage of Io's most colorful eruptions: (A) West of Zal; (B) Arinna; (C) Zamama; (D) Marduk and Dorian; (E) Pele, Babbar and Pillan; (F) Prometheus and Culann; (G) North Polar Ring; (H) Surt and Dazhbog.

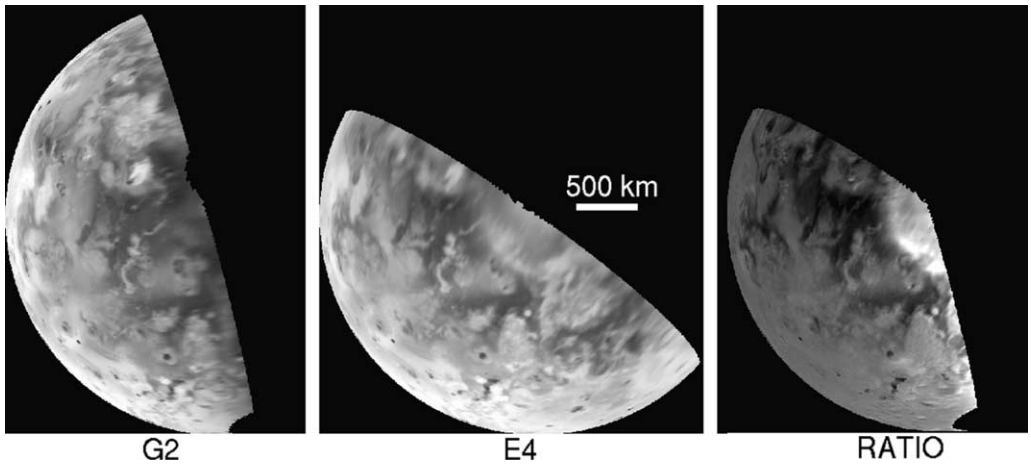

Fig. 5. Surface changes at the unnamed "North Polar Ring:" green filter images. A bright orange ring spanning nearly 900 km in diameter was emplaced prior to orbit E4 (see also color Plate 1, part G).

3.5. North Polar Ring

3.5.1. Description

The "North Polar Ring" refers to an eruption centered at ∼ 80° N, ∼ 100° W in a poorly imaged region near the pole. If not for the large extent of the deposit, the eruption may well have gone unnoticed. Ground-based monitoring (Spencer et al., 1997a) detected a short-lived, high temperature hot spot at high northern latitudes (70° ± 15° N, 35° ± 15° W), designated 9610A, on October 6, 1996, during the time span within which the ring must have been emplaced. This eruption was the first of a class of episodic, violent eruptions that took place at high northern latitudes during the Galileo mission.

3.5.2. Surface change

This singular event took place between orbits 2 and 4 (images 359986578 to 374575945) (see Fig. 5 and Plate 1G). Only longitudes from ∼ 65° W to ∼ 195° W can be seen in the orbit 4 image, but in the area covered, an apparently circular plume deposit was emplaced with a radius of 446 ± 15 km. The bright orange deposit reached nearly as far as Tvashtar and was centered within a few degrees of 80° N, 100° W. Assuming that the deposit was circular, the area affected was on the order of 625,000 km^2. The color of the deposit suggests that it was not wholly made up of SO_2 but instead included a sulfur component, as is common for the larger rings. The ring faintly persisted through orbit 14 but had vanished by the time of orbit 21, a little more than 2 years after it was emplaced.

3.6. Amirani

3.6.1. Description

Amirani (26° N, 115° W) is the site of the longest known active lava flows in the Solar System and one of the few volcanic centers on Io at which surface changes have been monitored by Galileo at high spatial resolution (see Section 4). Plumes from Amirani's lava flows were sighted at 2 locations by Voyager 1 (Strom and Schneider, 1982), and thermal emission from the region was clearly detected by Voyager's IRIS instruments (Pearl and Sinton, 1982). The eruptive center consists of a ∼ 300 km long, dark lava flow complex oriented roughly north–south. The lavas may derive from a vent near the middle of the flows or from a red-tinged patera to the southwest; in either case, the morphology and thermal signature of the flows seem to suggest insulated tube- or sheet-fed lavas (Keszthelyi et al., 2001). The northern end of the complex broadened noticeably between the Voyager flybys of 1979 and the first Galileo observations (McEwen et al., 1998a). High temperature hot spots were detected at Amirani by SSI during orbits 8, 10, 11, and 15 (McEwen et al., 1998a; Keszthelyi et al., 2001). A spatially-resolved thermal map made by NIMS on orbit 27 showed emission at several points along the flow complex, reaching a maximum temperature of at least 1000 K, along with thermal emission from the red patera to the southwest (Lopes et al., 2001). Sunlit plumes were seen over Amirani on orbits 4, 8, 21, and 22, and a diffuse auroral glow was seen over Amirani in an eclipse image from orbit 15 (Geissler et al., 1999a). This area is also apparently coated with forward-scattering frosts (Geissler et al., 2001b) that correspond to local enrichments in SO_2 abundance (Doute et al., 2001, 2003, in preparation).

3.6.2. Surface changes

Amirani was observed on 9 separate occasions in global monitoring images, during orbits 2, 4, 6, 7, 8, 9, 21, 22, and 29, and was also imaged twice at high resolution during orbits 24 and 27. Three major eruptions could be seen in the global images (Fig. 6). No changes were confidently detected over the interval between orbits 2 and 4 owing to the poor quality of the orbit 2 data. Between orbits 4 and 6 (images 374575922 and 383600826), a dark oval ring was emplaced, centered on 23° N, 115° W, with a mean radius of ∼ 200 km (180 km in the north–south direction and 220 km in the east–west direction). The dark spot at the cen-

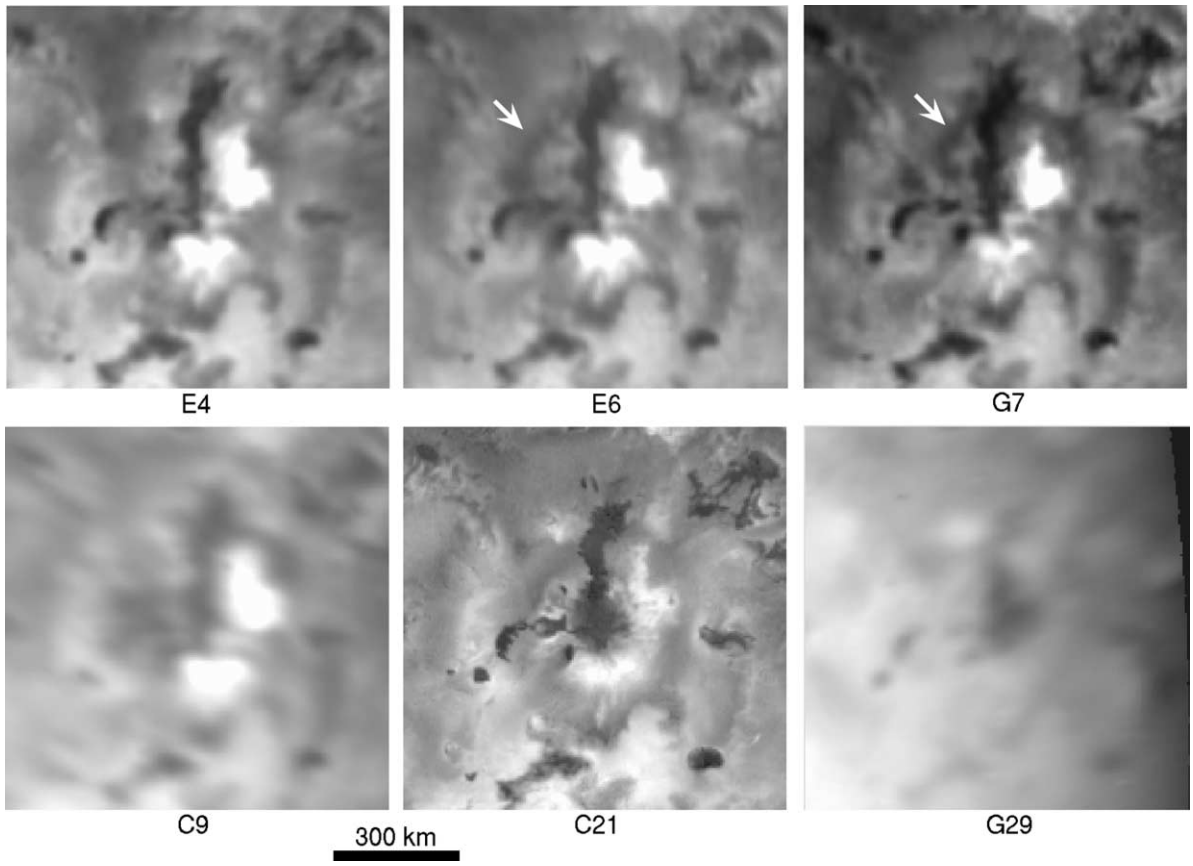

Fig. 6. Surface changes at Amirani: violet filter images. Arrows show a dark ring deposited by orbit E6 that was subsequently replaced by a smaller, more northerly ring before orbit G7. An active plume could be seen during orbit C21.

ter of the disturbance enlarged and there were changes in the bright deposits interior to the ring. The area coated by new materials was approximately 123,000 km^2. This event was immediately followed by another eruption that took place between orbit 6 and 7 (images 383600826 to 389654026), during which a smaller dark ring of radius 105–130 km was emplaced to the north of the previous deposit, the new ring centered on 24° N, 116° W. Other changes to Amirani's deposits may have taken place, but can not be distinguished from photometric variations in this case. A third major event took place between orbits 9 and 21 (images 401785407 and 506406118). A plume was visible in the orbit 21 image, and a new bright ring of 155 km radius had been emplaced to the southeast of the earlier eruptions (centered on 20° N, 116° W). The area affected was at least 70,000 km^2, not counting a possible dark ring exterior to the obvious bright deposit. Further changes were observed in the high-resolution images of orbits 24 and 27 (see Section 4), and a possible small eruption between orbits 21 and 29 can be seen in the global monitoring images (506406626 to 584334185) that emplaced new dark materials to the east of the lava flow (21° N, 112° W) to a maximum range of 75 km, covering an area of $\sim$ 10,000 km^2.

3.7. Tvashtar

3.7.1. Description

Tvashtar (63° N, 123° W) is a complex of eruptive centers situated in a chain of volcanic depressions known as Tvashtar Catena. These depressions (possibly calderas) include the largest known on Io, reaching dimensions of up to 177 km (Radebaugh et al., 2001). Tvashtar was the site of at least three known eruptions, including a spectacularly imaged eruption along a $\sim$ 25 km long fissure during orbit 25 that produced a fire-fountain of lava reaching 1 km in height (McEwen et al., 2000). This eruption was also observed from Earth by both the IRTF and Keck AO systems (Howell et al., 2001), which helped establish the duration ($\sim$ 36 h) and temperature (1300–1900 K) of the fire-fountaining event. The area was reimaged during orbit 27, when it was found that the fissure eruption had ended but new activity was taking place in the depression to the northwest of the depression with the fissure eruption (Keszthelyi et al., 2001). This activity included an extensive high-temperature flow and two smaller hot spots interpreted as possible vents (ibid.). Hot spots were again sighted during orbit 29 by both SSI and NIMS (Lopes et al., 2001), and a giant plume was detected by Cassini in both sunlit and eclipse observations (Porco et al., 2003). NIMS continued to detect thermal emis-

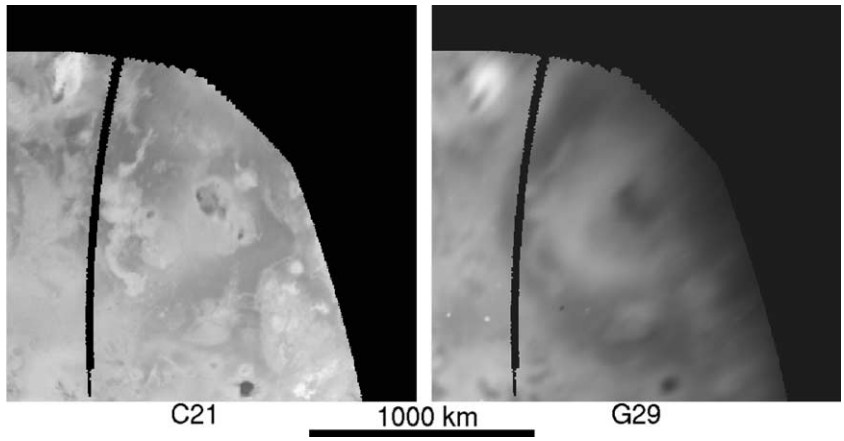

Fig. 7. Surface changes at Tvashtar: green filter images. Tvashtar's red ring was the most extensive of any plume deposit erupted during the Galileo Mission, covering over 1.5 million square kilometers.

sion from Tvashtar during orbits 31 and 32 (Lopes et al., 2003).

3.7.2. Surface changes

No signs of activity were seen at Tvashtar prior to the I25 eruption, even though the area was reasonably well imaged in orbits 2, 4, 6, 8, 9, 14, and 21. Even the dark deposits surrounding the orbit 25 fire fountain appear little changed from their configuration during orbit 21, although Wilson and Head (2001) infer from their symmetry and location with respect to the fissure that they were freshly deposited at the time of the fissure eruption. No regional or global color observations were made during orbits 25 or 27, so it is impossible to determine whether more extensive changes took place farther from the vents of these two eruptions. By the time of orbit 29, however, a giant red ring had been deposited around Tvashtar with dimensions that rivaled that of Pele (Fig. 7). The radius of the ring averaged ~ 720 km, but (like Pele's ring) it was elongated in the north–south direction so that it reached as far as 780 km toward the south. The width of the red band was approximately 275 km. In addition, new dark deposits were emplaced toward the southwest to a maximum extent of ~ 175 km and these were encircled by a bright ring approximately 300 km in radius. The total area affected covered by new deposits was at least 1,572,000 km^2, including 1,062,000 km^2 covered by the red ring alone.

3.8. "Thor"

3.8.1. Description

"Thor" (provisional name) (40° N, 135° W) refers to a large-scale eruption that occurred late in the Galileo mission in an area in which no previous activity had been reported. The best image of the area prior to the eruption showed only a poorly defined yellow spot that gave little indication that it was a sleeping giant. The region was imaged at high resolution after the eruption, during orbit 32, when a pair of new dark lava flows could be seen extending ~ 40 km from two different eruptive centers. Galileo captured an image of the erupting plume in daylight during orbit 31, when it set a record for the highest plume seen during any spacecraft observation of Io: dust particles could be detected as far as 500 km from the surface of the satellite. Also during orbit 31, NIMS detected a very prominent hot spot at this location that was given the temporary designation "I31A" (Lopes et al., 2003).

3.8.2. Surface change

This singular eruption took place between orbits 29 and 31 (images 584334185 and 615816245) and left a prominent bright ring around a new dark spot at 40° N, 133° W (Fig. 8). The ring is somewhat irregular in the low-resolution image from orbit 29 and its center appears offset from the dark deposit, at $\sim 39°$ N, 131° W. Its exterior radius is 298 ± 12 km, placing it among the largest of the white (presumably SO_2) rings on Io.

3.9. Arinna Fluctus

3.9.1. Description

Arinna Fluctus (32° N, 150° W) is a curvilinear fissure-like feature from which dark lava flows radiate in several directions, and is surrounded by bright frosts of SO_2 and red sulfur deposits. Thermal emission was observed by NIMS nearby at $36° \pm 6°$ N, $147° \pm 6°$ W that was ascribed to Arinna Fluctus (Lopes et al., 2001). Thermal emission from this location (designated 9606W) was also detected in ground-based observations in 1996 (Spencer et al., 1997a, cited by Lopes et al., 2001). No high-temperature hot spots were detected here by SSI, nor were any plumes seen by the imaging experiment. Arinna Fluctus was the site of minor Voyager-to-Galileo surface changes (Geissler et al., 1999b).

3.9.2. Surface changes

Three minor eruptions occurred at Arinna Fluctus that produced noticeable changes to the surrounding white and red deposits (Fig. 9). The area was imaged on orbits 2, 4, 6,

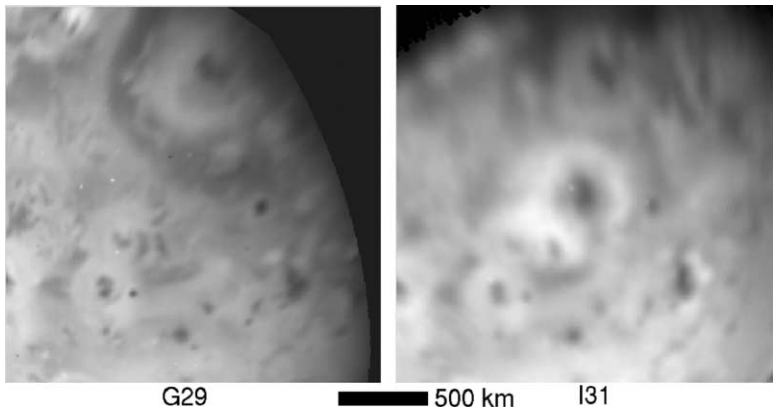

Fig. 8. Surface changes at Thor: green filter images. The bright deposits at Thor are the largest in their class, reaching nearly 300 km from the source vent.

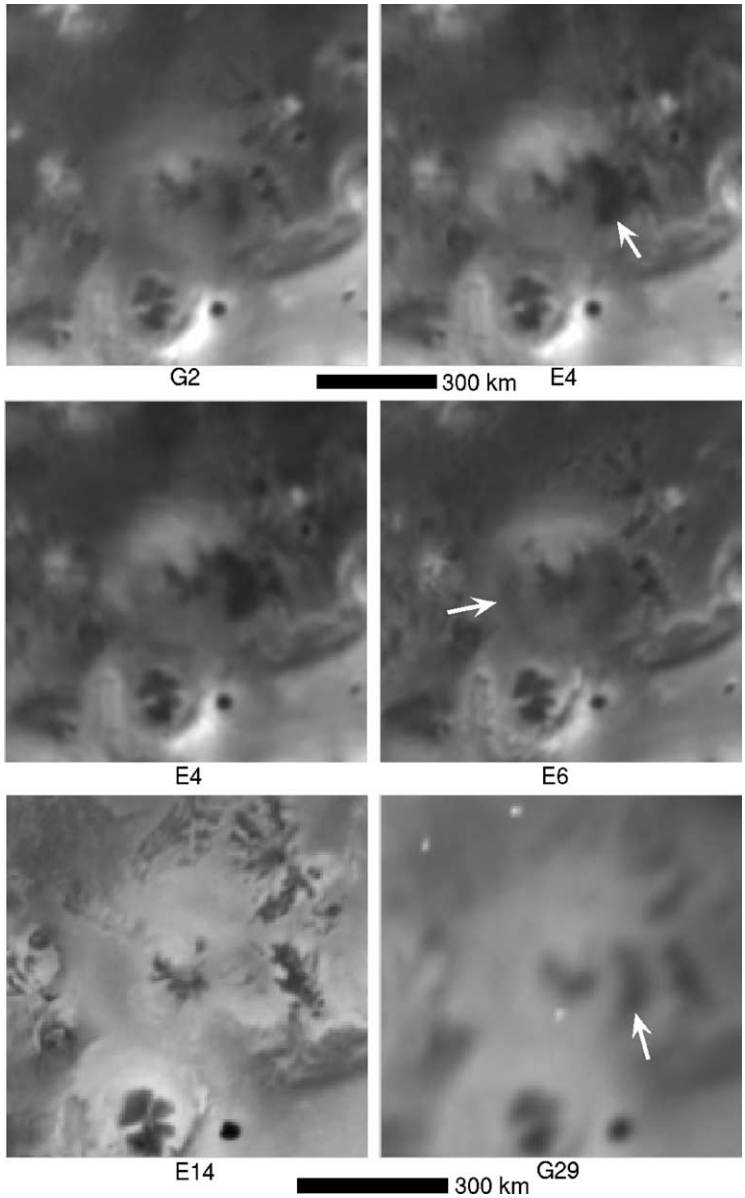

Fig. 9. Surface changes at Arinna: violet filter images. Arrows point out partial rings of dark (red) pyroclastic materials deposited during three minor eruptions. See also color Plate 1, part B.

7, 8, 9, 11, 14, 21, 29, and 31. Between orbits 2 and 4 (images 359986604 and 374575922), the ring around Arinna Fluctus enlarged and shifted to the northwest. New bright deposits were emplaced to the northwest, while new red materials were deposited to the east and northeast (see Plate 1B). The disturbance was centered at 31° N, 149° W and spread new materials as far as 200 ± 10 km from the source. The total area changed was 84,000 km^2. The eruption was followed immediately by another event that was less obvious because of the phase angle difference between the observations. Between orbits 4 and 6 (images 374575922 to 383655107), the plume deposit around Arinna Fluctus circularized, became more uniform, and attained a sharper margin. The ring darkened to the west but brightened to the east, as if the red deposits were buried by frosts of SO_2. The ring radius (200 km) and center (31° N, 149° W) remained unchanged, and the total area affected was ∼ 121,000 km^2. The final eruption ensued much later in the mission, probably between orbits 21 and 29 but definitely between orbits 14 and 29 (images 440873539 and 584334178). By the time of orbit 29, new red deposits were again emplaced to the east of Arinna Fluctus with a different distribution from that seen in orbit 4 and the refreshed ring was somewhat smaller than that during orbit 4 (radius 170 km). The total area covered by the smaller ring was ∼ 64,000 km^2.

3.10. Prometheus

3.10.1. Description

Prometheus (2° S, 155° W) is the source of Io's most persistently active plume, observed by both Voyagers and detected by Galileo at every favorable opportunity. Prometheus produces a dusty plume 50–150 km high that deposits a bright ring of SO_2 approximately 250 km in diameter, as well as fainter rings interior and exterior to the bright ring. Comparison of Voyager and Galileo images (McEwen et al., 1998a) showed that the center of the bright ring had migrated approximately 85 km to the west over the 20-year interval between spacecraft visits. The plume apparently derives from the distal end of lava flows issuing from a fissure on the south flank of Prometheus Patera. High temperature hot spots were detected during orbit 24 by NIMS both near the patera and along the dark flows to the west (Lopes-Gautier et al., 2000). Later NIMS observations from orbit 27 showed hot material along the entire length of the flows (Lopes et al., 2001). The flows have grown in length since the Voyager flybys and the plume source has either migrated along with them or shut off and later formed a new plume. A splash of red stains the area east of the patera, suggesting that sulfur-rich vapor emanated from the source of the silicate magma rather than from remobilization of surficial materials by lava flows.

3.10.2. Surface changes

Because of its incessant plume activity, surface changes near Prometheus were observed each time a pair of comparable images covered the region (Fig. 10). At least 6 distinct changes in radius or color of the circular plume deposits can be discerned in the Galileo images, and it is likely that others occurred but can not be distinguished due to photometric variations between image pairs. Prometheus' plume deposits are complex in structure, made up of several concentric rings caused either by variations in the vigor of the plume over time, or by the presence of more than one type

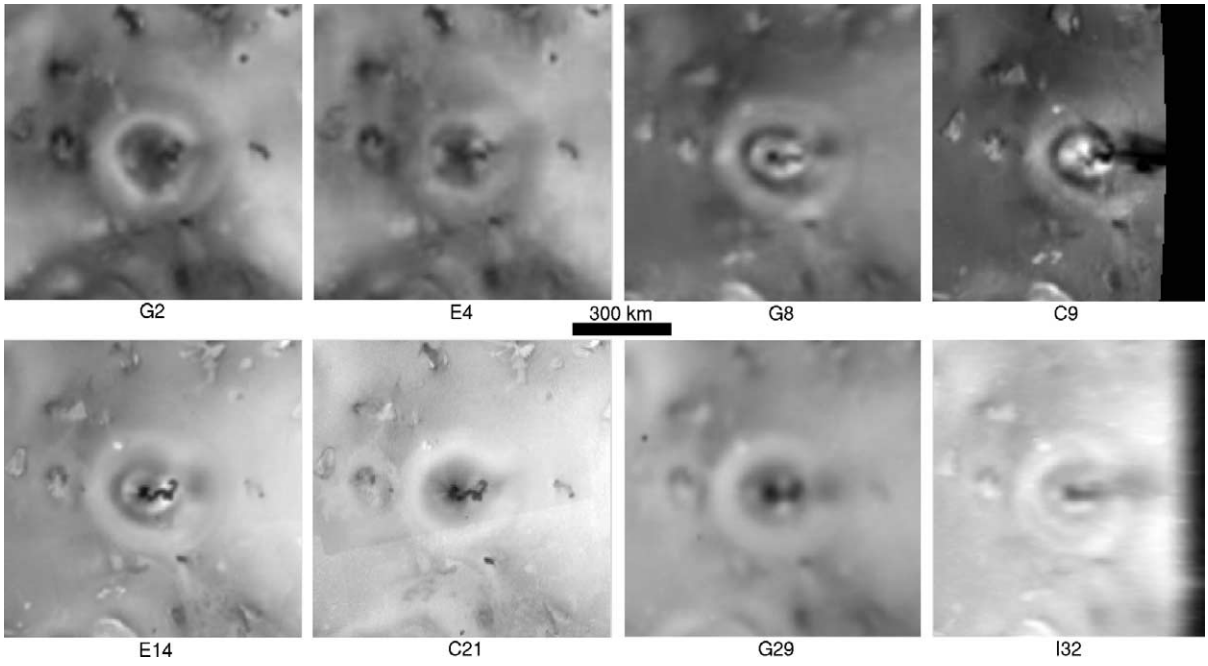

Fig. 10. Surface changes at Prometheus: violet filter images. Frequent changes near Io's "Old Faithful" plume showed that Prometheus remained active throughout the Galileo Mission.

of deposit from the same plume. For example, Zhang et al. (2002) point out that a plume may produce concentric shock annuli as the gas flow "bounces" over the surrounding plain, and the deposition pattern may be different at night from in daytime when a sublimation-driven atmosphere is present. Adding to the difficulty of image interpretation is the fact that the light-scattering properties of the various rings differ, so that some are more apparent at particular phase angles than others. The largest ring is quite invisible at low phase angles despite the fact that is apparent in spectral band-depth maps of SO_2 abundance, suggesting that it is made up of a thin veneer of fine-grained frost (Lopes-Gautier et al., 2000; Doute et al., 2001, 2003, in preparation; Geissler et al., 2001b).

The first noticeable change took place between orbits 2 and 4 (images 359986604 to 374575922) when the nearly circular ring darkened and enlarged and new bright deposits were emplaced inside the ring. The refreshed ring was 155 ± 5 km in radius, extending up to 175 km toward the east, and was centered at 1° S, 155° W. The total area changed (including everything within the enlarged ring) was 107,000 km^2 (see also Plate 1F). Radial spokes present in both the orbit 2 and orbit 4 images indicated that plumes were active during both these observations. A pair of higher-phase-angle green filter images acquired on orbits 8 and 9 (images 394478045 and 401863178) showed that the interior of the ring had changed and new dark deposits had been emplaced, particularly toward the east of the plume source. Given that the interior radius of the ring was $\sim$ 95 km, the area changed (within the ring only) was at least $\sim$ 22,000 km^2. The deposit was still centered at 1° S, 155° W. The plume itself cast a shadow that was visible as a dark streak to the east in image 401863178; its length (328 km) and the local incidence angle (73°) allow us to estimate the plume height at $\sim$ 100 km. Another small change was revealed by green filter images (401863178 to 420773065) between orbits 9 and 11. New bright deposits were emplaced within the dark, $\sim$ 100 km radius ring, and new dark deposits were emplaced on the ring itself, approximately 110 km to the north of the plume source. The total area changed, including the bright interior deposits and the dark deposits north of the dark ring, was just 28,000 km^2.

The detailed structure of Prometheus' rings was revealed during orbit 14, when a 6-color sequence was acquired that included image 440873539. At least 4 rings were present that were centered on the Galileo era plume source, plus the ghost of an older ring to the east that perhaps dated from Voyager times. The radii of these deposits were measured at 72 km (bright yellow), 95 km (dark), 125 km (white), and 200 km (a faint yellow ring that becomes prominent at high phase angles); the same structure can be seen in the 3-color sequence from orbit 8. The persistence of the easternmost relic ring fragment indicates that plume deposits can survive at least 18 months, since the start of the Galileo observations of Prometheus on orbit 2.

Photometric differences complicate the identification of surface changes between orbits 14 and 21 (images 440873539 to 506406626) (see Fig. 10). Moreover, radial spokes in both images indicate that plumes were active on these orbits. However, there are changes in the size of the prominent ring, the shape of the interior deposits, and the extent of the red deposits to the east that are diagnostic of genuine surface changes. The most prominent ring of orbit 14 (125 km radius) was replaced by a somewhat larger ring (130 km radius) that buried much of the red deposits to the east, out to a maximum range of 180 km. The bright deposits that radiate from the plume source also altered. The total area changed, as seen in the green filter images, amounted to 66,000 km$^2 \pm 20\%$. A similar figure was derived by comparing the orbit 14 images with those from orbit 29 (largely unchanged from orbit 21). It is likely that further changes took place between orbits 21 and 24, based upon comparison of images taken in two different colors (green images from orbit 21 and clear-filter images from the orbit 24 stereo sequence). However, it is clear that in the interval between orbits 21 and 29 (images 506406626 to 584334185), the prominent ring around Prometheus broadened and its outer margin sharpened in contrast with a yellow outer ring of radius 195 ± 10 km. The area changed (including everything within this outer ring) amounted to 126,000 km^2. The final change occurred between orbits 29 and 32 (images 584334185 and 625664901), when a smaller gray ring of radius 140 km was emplaced around the plume source, particularly noticeable in the violet filter images from orbit 32; the area affected (within the small ring) amounted to just 65,000 km^2.

3.11. Culann

3.11.1. Description

Culann (20° S, 159° W) was the site of surface changes noted even prior to the arrival of Galileo (Spencer et al., 1997b). Conspicuous Voyager-to-Galileo surface changes led McEwen et al. (1998a) to conclude that Culann was the site of ongoing activity. The eruptive center is made up of dark lava flows adjacent to asymmetric bright red deposits, and the entire region is surrounded by forward-scattering frosts of SO_2 that are visible in high-phase-angle SSI images and in NIMS compositional maps (Doute et al., 2001 and 2003, in preparation; Geissler et al., 2001b). Small plumes were sighted over Culann by Galileo SSI in orbits 1 and 2 but significant nondetections were made in orbits 7, 8, and 9 (McEwen et al. op. cit.). Gas-rich plumes were again identified in eclipse imaging during orbit 15 (Geissler et al., 1999a) but no dusty plumes were seen during orbits 21 or 22 (Keszthelyi et al., 2001). Hot spots were detected by NIMS early in the mission during orbits 1, 2, and 3, but NIMS did not detect thermal emission during orbits 6 and 7; NIMS detected emission from the lava flows west of Culann again during orbits 8, 9, and 10 (Lopes-Gautier et al., 1999), and later orbits including I32 (Lopes et al., 2003).

A high-temperature hot spot was seen by SSI during orbit 11 (Keszthelyi et al., 2001).

3.11.2. Surface changes

Distinctive surface changes occurred at Culann early in the Galileo mission, followed by several more subtle changes (Fig. 11). The most obvious changes took place between orbits 2 and 4 (images 359986604 to 374575922; see Plate 1F). This eruption left expanded red deposits to the east of Culann, new bright deposits to the south, and a distinct ring that was visible to the north and west. The radius of the ring fragment was 210 km if it was derived from the source of the red deposits or ∼ 165 km if derived from western part of dark flow. The total area changed was 131,000 km^2. Photometric variations complicate the identification of changes between orbits 4 and 6 (images 374575922 and 383655107) but several subtle changes were probably real: new bright deposits were emplaced to the north, southeast, and west; the dark margin of the northern bright deposits moved northward; and the ring arc to the northeast extended further to the south. The area changed was 124,000 km^2. No changes were observed between orbits 6 and 9, consistent with the lack of plume or thermal activity, and only small changes took place between orbits 9 and 11 (images 401863178 and 420773065) when new white deposits were emplaced to the south, at the western margin of red deposits, that covered an area of only 7,000 km^2.

Two other minor changes around Culann took place late in the mission. Between orbits 14 and 21 (images 440873539 and 506406626), new red deposits were emplaced to the north, close to the source (out to a maximum distance of 75 km), affecting an area of just 7,000 km^2. More extensive red materials were deposited to the southeast of Culann between orbits 21 and 29 (images 506406626 and 584334185) out to a maximum range of ∼ 175 km; the area changed amounted to 23,000 km^2.

3.12. South Polar Ring (Illyrikon Regio)

3.12.1. Description

The "South Polar Ring" (70° S, 170° W) refers to a previously unnoticed eruption in Illyrikon Regio, a region poorly imaged by Galileo and in darkness during the flyby of Voyager 1. There are no reports of plumes or hot spots in this area, which is well separated from the nearest NIMS candidates (Sethlaus 50° S, 195° W and Gabija 52° S, 204° W) and on the opposite side of Io from the southernmost Voyager IRIS hot spots. In view of the fact that several large scale eruptions took place at high northern latitudes during

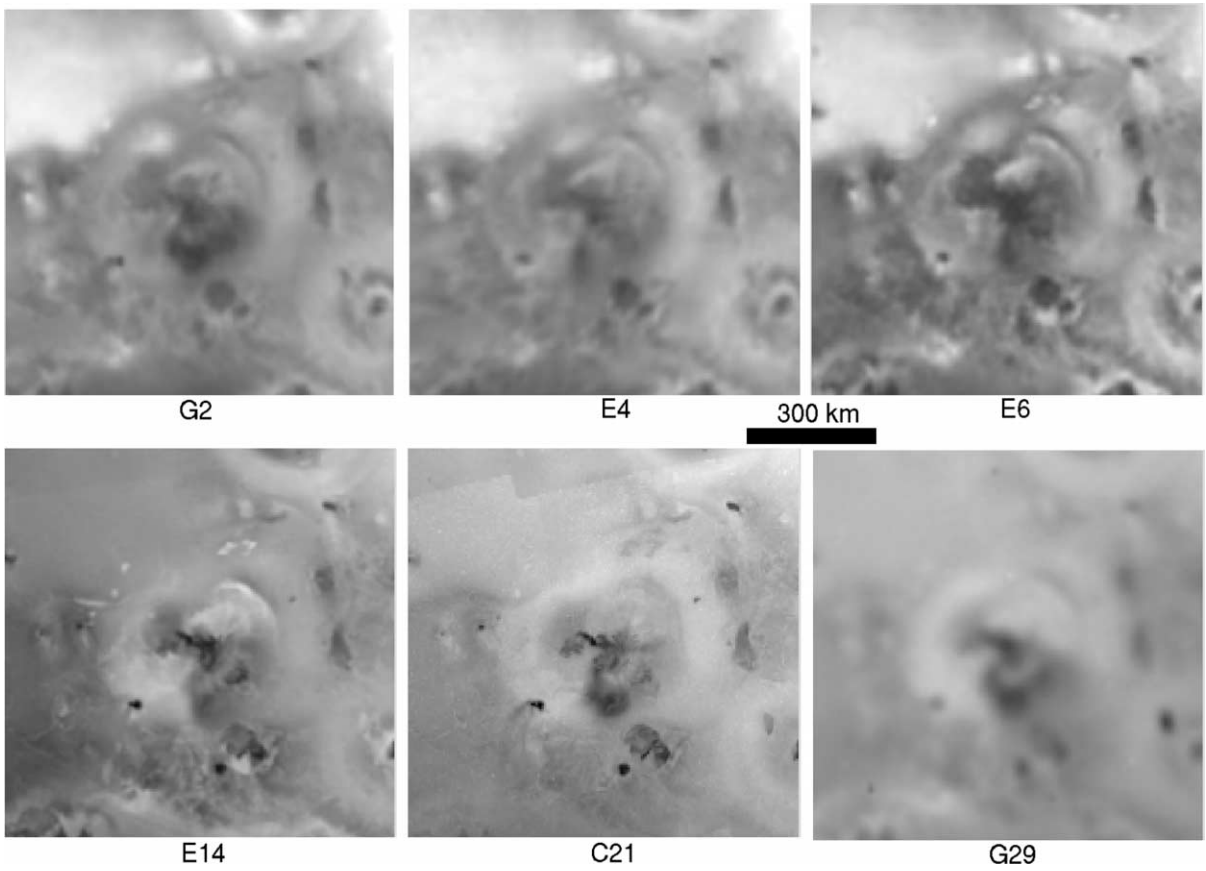

Fig. 11. Surface changes at Culann: violet filter images. Several subtle changes in the red (dark) and white (bright) materials surrounding Culann were apparent, particularly early in the Galileo Mission. See also color Plate 1, part F.

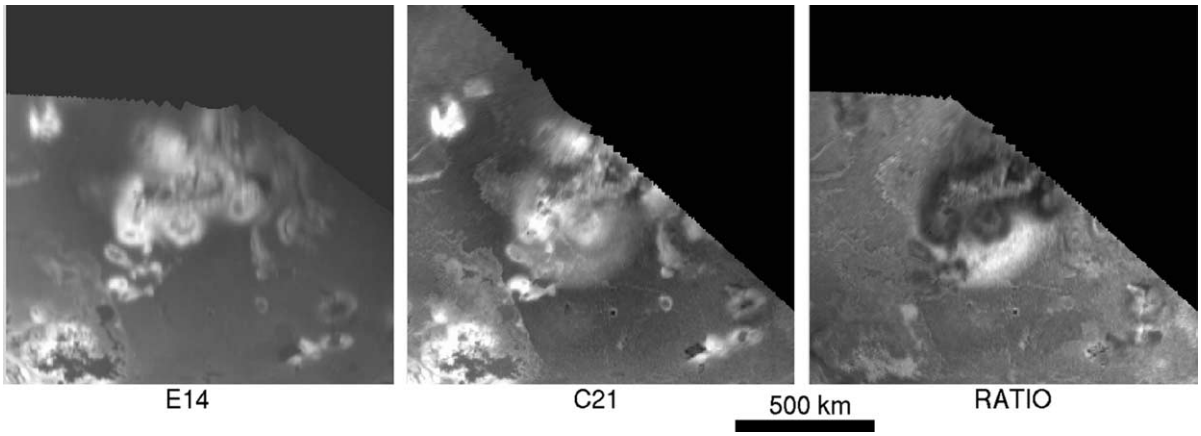

Fig. 12. Surface changes at the "South Polar Ring:" violet filter images. This small gray ring erupted from an unnamed patera near the South Pole, brightening the nearby dark plains and darkening the surrounding SO_2 deposits.

the Galileo mission, the relative lack of activity near Io's south pole is curious.

3.12.2. Surface change

A singular eruption took place in Illyrikon Regio between orbits 14 and 21 (images 440873652 to 506406118). Both violet and green filter images show a definite circular ring around an $\sim$ 80 km diameter caldera at 70° S, 170° W that was formerly surrounded by a small white rim (Fig. 12). The new ring appeared gray in color pictures, darkening the nearby bright deposits and brightening the dark plains, and had a radius of 237 ± 7 km. Prior imaging of the area during orbits 2, 4, 6, and 8 showed no previous changes, but the new deposit persisted through orbit 29 (image 584334178). The total area covered by the eruption was 190,000 km^2.

3.13. Zamama

3.13.1. Description

Zamama (18° N, 174° W) is a Galileo-era eruption site that was apparently inactive during the Voyager visits (or buried by deposits from nearby Volund) but was already very active by the time of Galileo's earliest imaging observations, as shown by the presence of a plume, high-temperature SSI hot spot, and significant post-Voyager surface changes starting with orbits 1 and 2 (McEwen et al., 1998a). High-resolution views acquired during orbit 32 show a shield-like structure with dark lava flows extending $\sim$ 150 km to the east. No plume was detected during orbit 7, but plumes were later spotted in orbits 8, 11, and 14 (McEwen et al., 1998a; Keszthelyi et al., 2001) and auroral glows from the region were seen in orbits 11, 14, and 15 (Geissler et al., 2001a). Plume activity had apparently diminished by the time of orbits 21 and 22, when significant nondetections of Zamama's plume were made by SSI (Keszthelyi et al., 2001). Forward-scattering frosts are also apparent in this region (Geissler et al., 2001b). NIMS detected thermal emission from Zamama during the first three orbits that indicated temperatures consistent with basaltic or ultramafic volcanism (Davies et al., 1997) but did not detect emission during orbits 6, 7, 8, or 9; a detection was again made during orbit 10 (Lopes-Gautier et al., 1997). Later NIMS observations detected Zamama during orbits 24 and 32 (Lopes et al., 2001, 2003).

3.13.2. Surface changes

Three notable surface changes were observed at Zamama by Galileo SSI along with several other smaller eruptions. The most prominent eruption took place between orbits 2 and 4 (images 359986604 to 374575922; see Fig. 13 and Plate 1C). A new, irregular bright ring was emplaced around the dark, central lava flows with a radius of $\sim$ 185 km, centered on the lava flows at 18° N, 171° W; new dark deposits were also emplaced toward the north and northwest, out to a maximum range of 250 km. The total area changed was 136,000 km^2. This eruption was immediately followed by a second surface change between orbits 4 and 6 that is more difficult to discern because of photometric variations. During this event (images 374575922 to 383655107), the central dark deposit broadened at its western side and new bright deposits were emplaced along the margins of the lava flows. It is possible that new bright SO_2 deposits were emplaced toward the north and northwest of the eruptive center but these may simply be more obvious in the orbit 6 data and cannot be definitively distinguished because of the aforementioned photometric differences. The total area affected by the eruption (not including the exterior bright deposits) was 37,000 km^2. No changes took place between orbits 6 and 8, but a faint ring appeared before orbit 9 that was 140 ± 5 km in radius. The third large eruption took place between orbits 9 and 14 (images 401863204 to 440873652). Zamama's plume was actively erupting during orbit 14 and new deposits surrounded the lava flow, including a refreshed bright ring that had enlarged to 150 ± 5 km, again centered on the lava flows to the east of the eruptive center. New bright red deposits were emplaced to the west of Zamama along with new white materials that were deposited inside the ring to the north of the lava flow. The area affected was $\sim$ 96,000 km^2. More subtle changes occurred between orbits 14 and 21 (im-

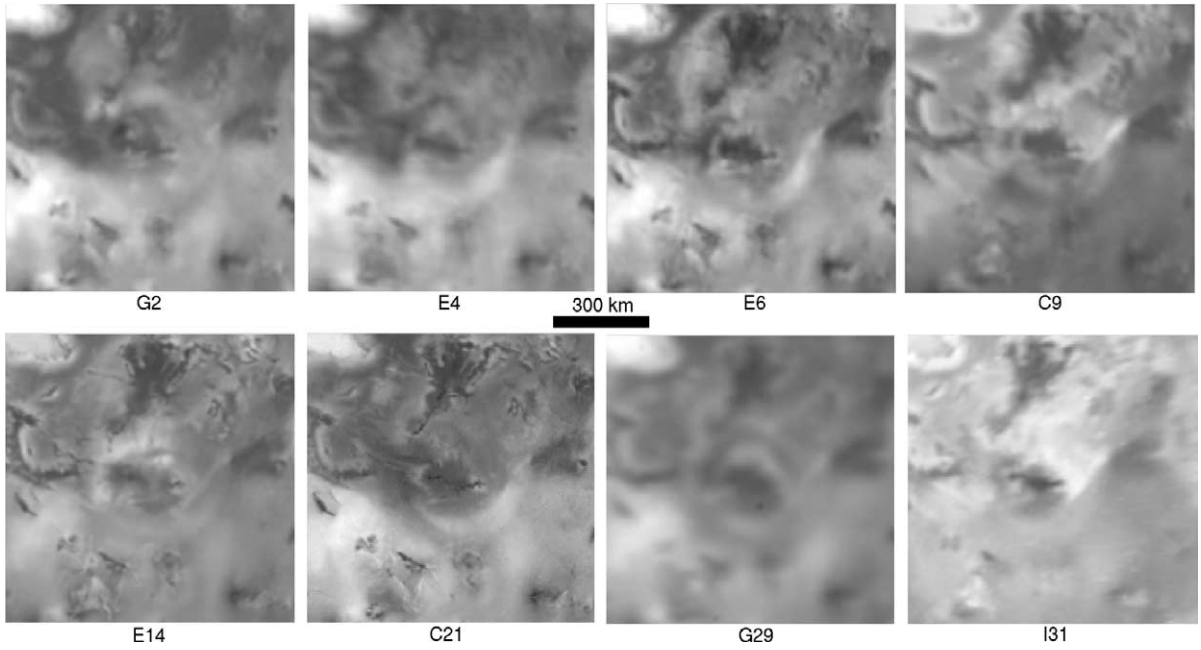

Fig. 13. Surface changes at Zamama: violet filter images. Changes can be seen in the central dark deposits (silicate lava flows), the red deposits west of the vent, and the distant ring fragments surrounding this persistently active volcano. See also color Plate 1, part C.

ages 440873652 to 506406118): extensive new red deposits erupted from the silicate source at the west end of the flow field, reaching a maximum distance of 170 km, and a small white deposit appeared near the source of the red materials. The white deposits to the north of the volcano faded (were buried, altered or eroded), and the deposit around the lava flows contracted and circularized. The area that changed was $\sim 65{,}000$ km^2. A new bright ring appeared between orbits 21 and 29 (images 506406118 to 584334178) that was centered at 18° N, 172° W and had a radius of 140 ± 5 km radius, affecting an area of 62,000 km^2. A final small eruption may have occurred between orbits 29 and 31 (images 584334185 to 625664901) that produced minor changes to the dark deposits to the south and the red deposits to the west, affecting an area of just 14,000 km^2.

3.14. Marduk and Dorian

3.14.1. Description

Marduk (27° S, 209° W) is another persistently active volcanic center, the site of plumes and hot spots during the Voyager flybys and prominent Voyager-to-Galileo surface changes that were observed by HST even prior to Galileo's arrival (McEwen et al., 1998a). The highest-resolution image of the volcano was taken by Voyager 1 but since that time new dark lava flows have erupted toward the northwest, forming Marduk Fluctus, and new red deposits were emplaced to the southeast. Sunlit plumes have been spotted by SSI over Marduk during orbits 6, 8, 11, and 21 (McEwen et al., 1998a; Keszthelyi et al., 2001) and auroral emissions from the region were seen in orbits 6, 9, 10, and 21 (McEwen et al., 1998a; Geissler et al., 2001a). SSI detected high temperature thermal emission from a pair of hot spots during orbits 1 and 9 (McEwen et al., 1998a) while NIMS observed thermal emission from Marduk at each opportunity from orbits 1 to 10 (Lopes-Gautier et al., 1997) and during favorable opportunities afterward (R. Lopes, personal communication, 2003).

To the south of Marduk is a prominent mountain massif known as Dorian Montes, estimated to reach at least 7.7 km in height (Schenk et al., 2001). It was imaged at moderate resolution during orbit 24, but at such a high sun angle that little of its topography could be seen (Turtle et al., 2001). It is a plateau roughly 200×100 km in size and, like many Ionian mountains, is surrounded by a bright halo of SO_2. Marduk and Dorian are particularly bright at high phase angles, indicative of forward-scattering frosts (Geissler et al., 2001b).

3.14.2. Surface changes

Interpretations of Galileo imaging observations of this region are greatly complicated by variations in illumination and viewing conditions between successive pairs of images, coupled with marked local variations in surface scattering properties. At least three eruptions can be identified at Marduk (Fig. 14), while several others likely occurred but cannot be distinguished from photometric variations. The first major explosive eruption took place between orbits 2 and 6 (images 359986604 to 383655107). New dark deposits were emplaced to the west of the Marduk Fluctus lava flows and a broader and more complete bright ring appeared around the lava flows, centered at 24° S, 211° W with a radius of

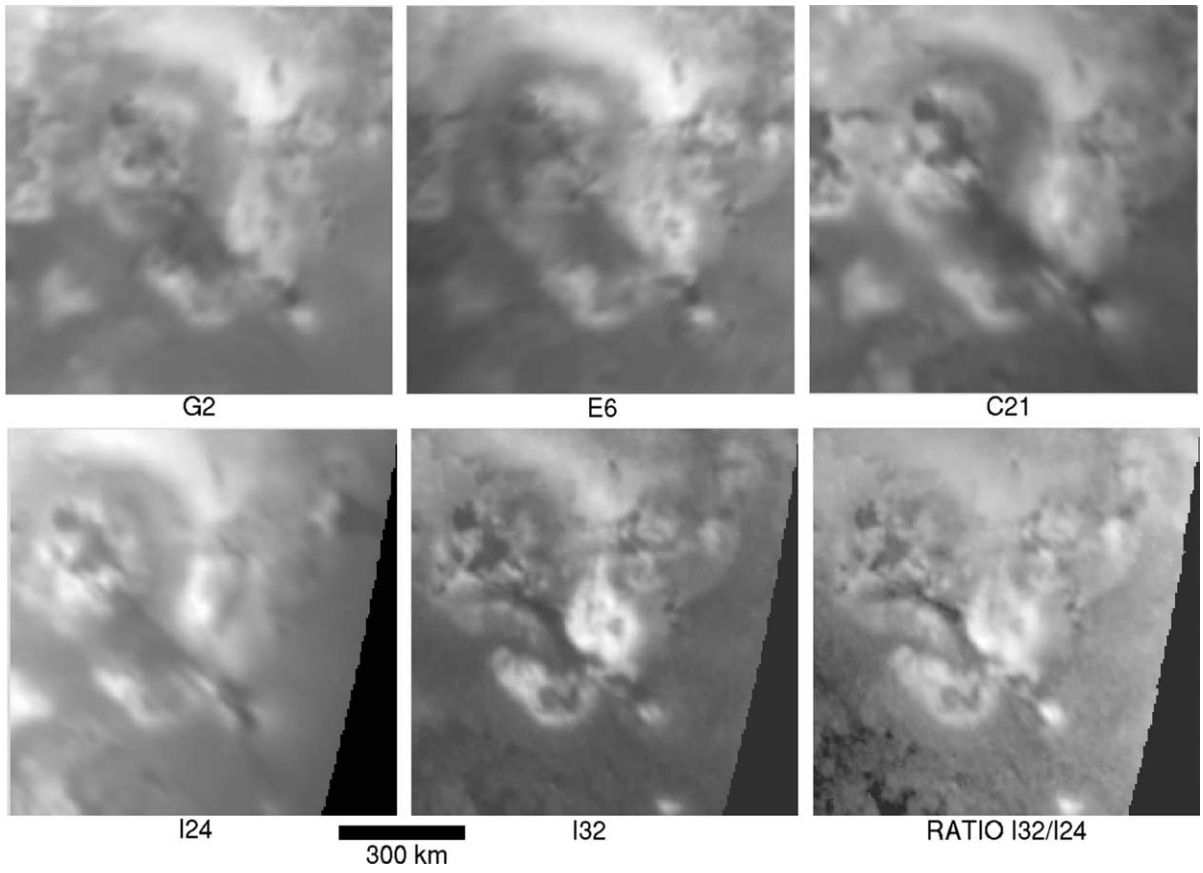

Fig. 14. Surface changes at Marduk and Dorian: violet filter images. Changes in the vague ring around Marduk and in the red pyroclastic deposits southeast of the vent were evident early in the Galileo Mission. Later, bright materials were emplaced around the Dorian Montes mountains that partially covered the older red deposits. See also color Plate 1, part D.

250 ± 20 km. New bright deposits appear to the southwest of the volcanic center and to the west of the red materials to south. The maximum range of the deposition, from the silicate source to the end of red deposits (presumably refreshed when the adjacent bright materials were deposited) was ~ 270 km, and the total area changed during the eruption was 177,000 km^2. A second period of activity followed in the interval between orbits 6 and 21 (images 383655107 and 506492200). It is likely that there were two eruptions during this period, one between orbits 4 and 8 and another between orbits 8 and 21, but we can not be certain of these. Sometime between orbits 6 and 21, the ring around Marduk Fluctus darkened, filled in and shifted on the east side but brightened on the west side. The brightness variations could be photometric effects, but the shape changes are not. New circular bright deposits surrounded the lava flows, out to a radius of 115 ± 5 km, that were centered on 23° S, 211° W. The outer dark ring was 210 ± 10 km and the total area changed was 132,000 km^2. A third distinct eruption occurred between orbits 21 and 24 (images 506492200 and 520873426) when a new dark yellow ring was emplaced around the lava flows, centered at 25° S, 212° W and 208 ± 5 km in radius. The bright materials adjacent to the lava flows also altered and the red deposits to the south darkened out to a maximum distance of ~ 250 km. The area affected was 149,000 km^2, of which 18,000 km^2 were the refreshed red deposits.

Only minor changes ensued between orbits 24 and 29, affecting the white deposits to the northeast, but two interesting events took place near Marduk and Dorian between orbits 24 and 32, probably between orbits 29 and 32 (see Plate 1D and the ratio image in Fig. 14). First, a dark red linear feature extended southwards from the silicate source vent for a distance of over 100 km, broadening in the direction away from the vent. Because of its sharp margins and straight linear planform, we suggest that this was a new lava flow rather than a pyroclastic deposit. Its red color could have been caused by a surficial paint of red sulfur or it may mean that the flow itself was made up of sulfurous materials. The second notable change during this period was a brightening at the base of Dorian Montes, the mountain massif to the southeast of Marduk's red deposits. An earlier brightening here (between orbits 6 and 8) may have been due to photometric effects, but this event produced new bright deposits that clearly overprinted existing red pyroclastic deposits. Similar to Zal Montes and Haemus Mons, discussed earlier, we interpret this as an episodic seepage of SO_2 that flowed from the base of Dorian and out onto the surrounding terrain.

3.15. Kaminari

3.15.1. Description

Kaminari (Kami-Nari, 8° S, 234° W) is a dark patera ~ 30 km across that produced a small eruption notable only because it disturbed the dark deposits from nearby Pillan. Although it was clearly active, neither NIMS nor SSI detected Kaminari as a hot spot, perhaps because of faint emission (low temperatures or small hot areas) and inadequate spatial resolution.

3.15.2. Surface changes

Kaminari signaled its activity as early as orbit 10 by rapidly clearing itself of debris after Pillan's eruption; the patera and a small ring of white materials covering less than 2,000 km^2 can be seen peeking out from under the dark ash in the first images taken after Pillan's eruption (e.g., image 413744204). The largest eruption took place between orbits 11 and 21 (images 420832945 to 506501100) but is better seen by comparing the green filter images from orbits 10 and 21 (Fig. 15). This event produced a small bright ring 92 ± 5 km in radius that was centered at 9.7° S, 233° W and surrounded a diffuse dark deposit, affecting an area of 48,000 km^2. Further activity was evident between orbits 21 and 24 (images 506492200 to 520873452), when new bright deposits were emplaced to the west of Kaminari (and also some toward the north). These noncircular deposits overprinted the darker Pillan ash, reaching a maximum range of ~ 150 km from Kaminari, and covered an area of ~ 15,000 km^2.

3.16. Pillan

3.16.1. Description

The explosion near Pillan (12° S, 244° W) during orbit 9 was in some ways Io's most dramatic eruption. It was witnessed by both Galileo and HST, setting a record for the highest temperature lavas observed erupting anywhere in the Solar System, and produced a conspicuous "black eye" on the distinctive red deposits from nearby Pele. Its thermal emission and high-resolution morphology have been studied in detail to gain clues about the nature of the eruption. Apparently inactive during the Voyager flybys (except for a possible darkening between Voyagers 1 and 2; McEwen, 1988) and unchanged from its 1979 appearance at the start of the Galileo mission (McEwen et al., 1998a), Pillan was detected as a hot spot by NIMS at every favorable opportunity from orbit 2 onward (Lopes-Gautier et al., 1997, 1999). SSI saw no high temperature hot spot on orbits 1 or 6, but NIMS data indicate that an eruption was already underway by orbit 8 (Davies et al., 2001). Both instruments monitored Pillan's thermal emission during orbit 9 and the combined measurements suggested that the lava temperatures reached at least 1870 K, indicative of an ultramafic composition (McEwen et al., 1998b). At the same time, plumes were spotted over Pillan by both SSI and HST (McEwen et al., 1998a; Spencer et al., 1997c) that reached 140 km in height and were seen again in orbit 10. Subsequent imaging observations showed that the eruption arose from a linear fissure system to the northeast of Pillan Patera, from which a total of ~ 3100 km^2 of lava issued prior to orbit 10 (Keszthelyi et al., 2001; Williams et al., 2001). Continued thermal observations from orbit 10 onward showed a steady decline in both the temperature and power emitted from the volcano, consistent with the spreading and cooling of lava flows (Davies et al., 2001).

3.16.2. Surface changes

Phillips (2000) gives a detailed description of the surface changes associated with Pillan. Pillan gave some warning signs of an impending eruption prior to orbit 9, in the form of changes to the brightness and color of its caldera. Pillan patera darkened noticeably between orbits 1 and 2 (images 349673952 to 359986578) and later brightened between orbits 2 and 6 (images 359986578 to 383758500) and again between orbits 6 and 8 (383758500 to 394552445). Although Pillan is within the range of Pele's pyroclastic deposits, the brightenings of Pillan were not simply due to mantling by

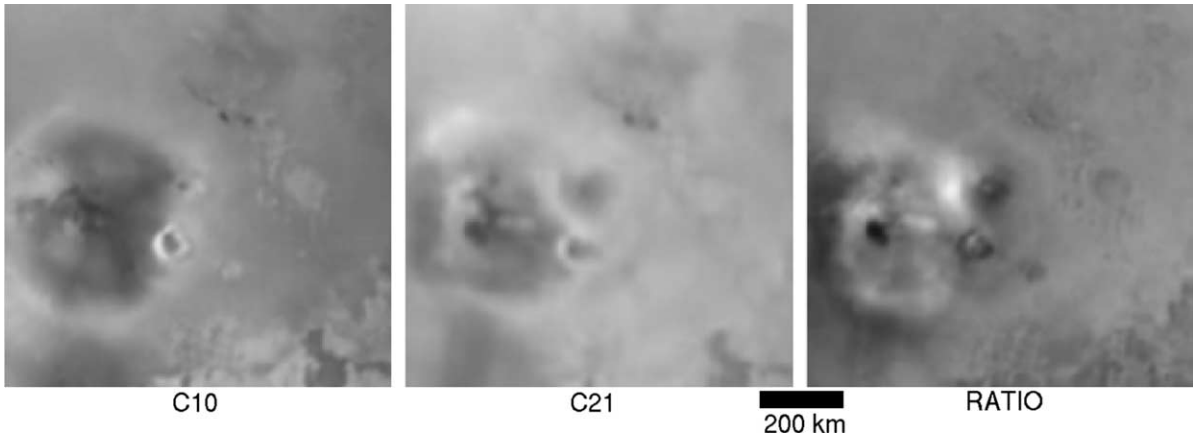

Fig. 15. Surface changes at Kaminari: green filter images. Kaminari (at the center of the picture) darkened and was surrounded by a small, bright ring between C10 and C21.

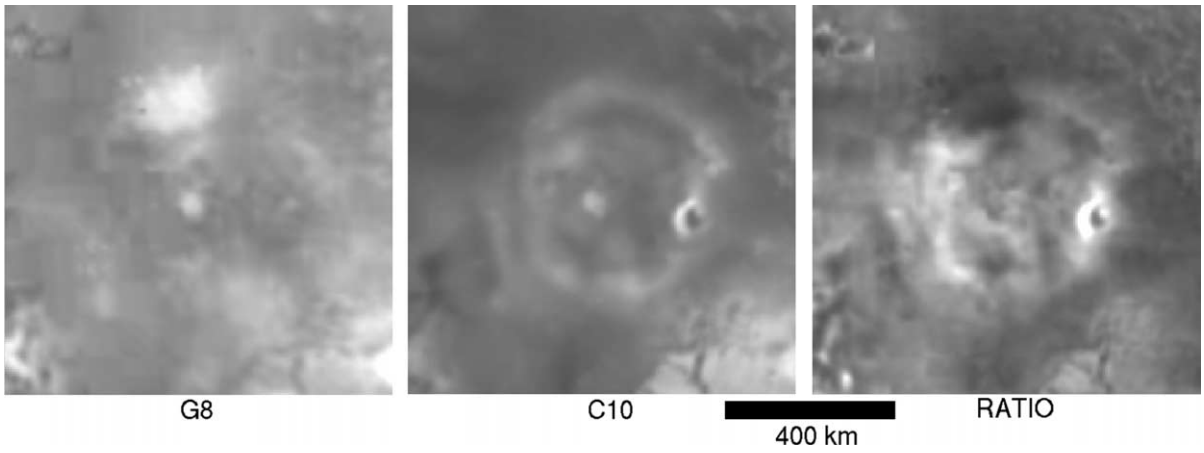

Fig. 16. Surface changes at Pillan: violet filter images. Before-and-after views of the eruption of black, silicate-rich pyroclastic deposits at Pillan. Also shown is the small white ring around Reiden Patera, at the eastern edge of Pillan's dark deposits. See also color Plate 1, part E.

fallout from Pele because they lacked the characteristic color of Pele's red ring. Instead, they were likely due to flooding the caldera with bright SO_2 or perhaps caused by alteration of red materials to a more neutral color. Pillan's eruption occurred during orbit 9 and is spanned by images acquired in orbits 8 and 10 (images 394519123 to 413744204; Fig. 16 and Plate 1E). The explosion emplaced a quasicircular dark deposit 245 ± 10 km in radius, centered on the lava flows at 11° S, 242° W. The dark deposit was surrounded by a bright rim 35 km wide, and was flattened towards the west by interference with Pele (active at the same time). The area covered by new deposits, including the bright rim, was $\sim 205{,}000$ km^2. SSI multispectral measurements showed a shallow absorbtion at 0.9 μm in the dark deposits, suggesting that they were made up of silicate ash (Geissler et al., 2000). The region remained unchanged between orbits 10 and 11 but the caldera darkened again before orbit 21, likely by the time of the orbit 14 observations. The darkening of Pillan patera after orbit 11 (shown in the Kaminari illustration, Fig. 15) is attributed by Keszthelyi et al. (2001) to flooding of the caldera with lava erupted from the fissure system, ~ 60 km to the northeast. Only minor changes occurred to Pillan after orbit 14, associated with burial by Pele or the eruption of nearby Kaminari. A bright deposit that reappeared on a broad plateau to the north of Pillan before orbit 21 was suggested by Phillips (2000) to have been caused by episodic seepage of SO_2 from the adjacent unnamed mountain. Pillan's deposits were almost completely disguised by orbit 29, little more than 3 years after their eruption.

3.17. Pele

3.17.1. Description

Pele (19° S, 258° W) is one of Io's most distinctive volcanoes, owing to its giant plume, enormous red ring and consistent high-temperature thermal emission. The highest resolution daytime image of Pele was taken by Voyager 1 and shows a dark, 24 km diameter caldera at the base of the Danube Planum plateau. It was the source of a 300 km high plume and a high-temperature hot spot during the Voyager flybys and was detected by ground-based thermal observations during the 1980s and 1990s at intensities up to the level seen by Voyager 1 (Spencer and Schneider, 1996). Pele is among the brightest sources of short wavelength (~ 1 μm) thermal emission and has been regularly seen in eclipse images taken by Galileo and Cassini. Nighttime images of Pele taken by SSI showed a curved line of hot spots interpreted to be glowing lava at the edge of a lava lake, similar to (much smaller) terrestrial lava lakes. Temperatures in these freshly exposed lavas were estimated to be 1760 ± 210 K (Lopes et al., 2001) and subsequently measured at 1300–1800 K by Radebaugh et al. (2004). Detailed modeling of Pele's infrared spectrum suggests that little thermal emission is contributed by expanses of cooling lava, and the consistency of its thermal emission, high temperatures and lack of a large cooling component are all consistent with the interpretation of Pele as a long-lived, stable but active lava lake (Howell, 1997; Davies et al., 2001). Modeling of SSI eclipse observations suggested a reduced area of high-temperature lava during orbits 6 and 9 (McEwen et al., 1998a), while NIMS observations indicated reduced activity during orbit 8 (Davies et al., 2001).

Post-Voyager detections of Pele's plume have been problematic, in part because of the insensitivity of Galileo's SSI camera to ultraviolet wavelengths. HST detected plumes in 1995 and 1996 (Spencer et al., 1997b) and again in July, 1997, between Galileo orbits 9 and 10 (Spencer et al., 1997d). SSI failed to detect a plume at Pele during orbits 1, 2, 6, 9, 21, and 22, even when extended exposures were acquired in orbits 6 and 9, and made only a marginal detection of a 460 km high plume during orbit 4. Cassini detected a large sunlit plume over Pele when it imaged Io in the near-ultraviolet during Galileo's orbit 29.

3.17.2. Surface changes

Despite the absence of obvious plumes, surface changes show that plume deposition altered or replenished Pele's red

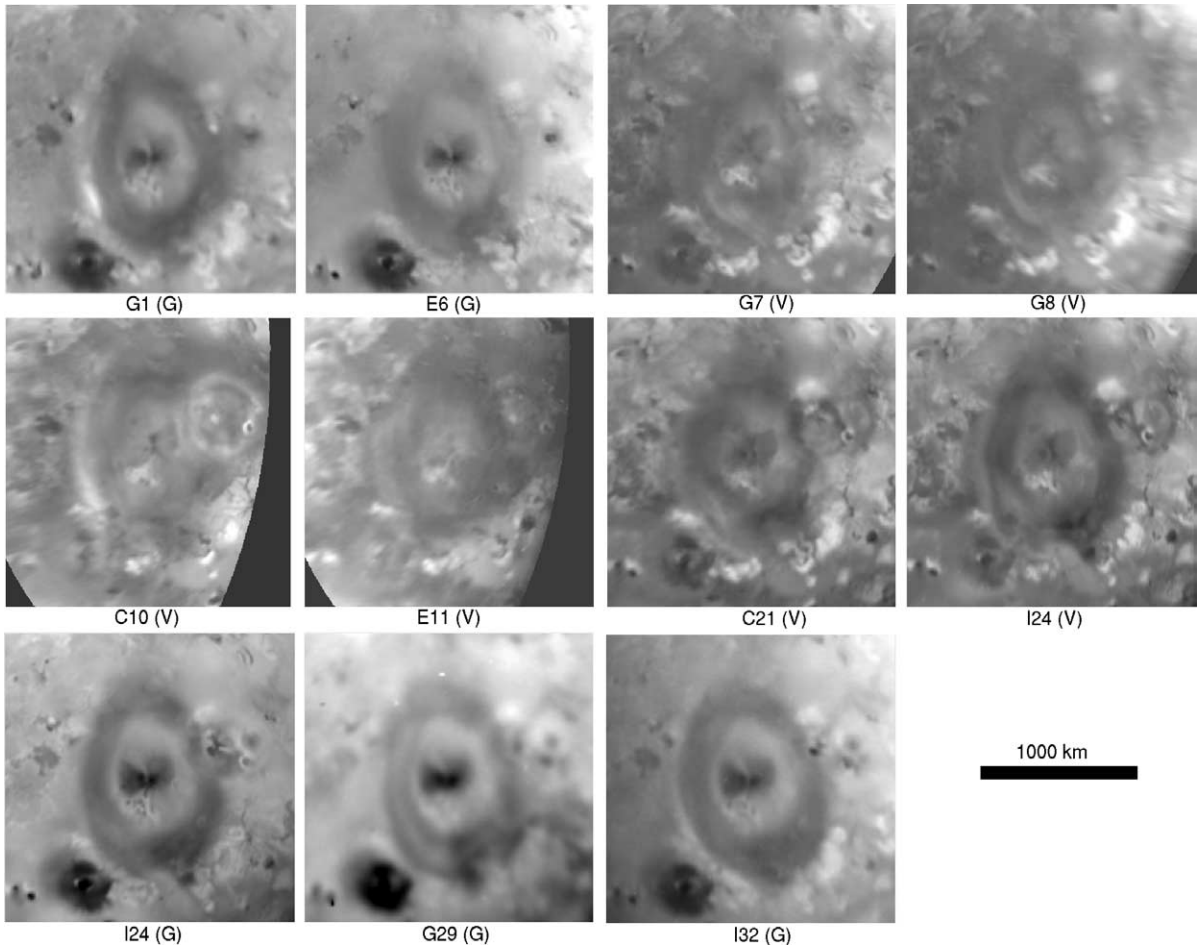

Fig. 17. Surface changes at Pele: green (G) and violet (V) filter images. See also color Plate 1, part E.

ring during every interval except perhaps between orbits 6 and 7 (Fig. 17). Prior to orbit 10, these changes were manifested by subtle differences in brightness and shape that could easily be taken for photometric effects. However, Pillan's eruption during orbit 9 provided a convenient marker throughout the latter part of the mission, whereby Pele's activity could be unambiguously documented as Pillan's dark ash deposits were gradually buried by red fallout from Pele. The first of the pre-Pillan changes took place between orbits 1 and 6 (Pele was too close to the limb during the orbit 2 observation to enable a useful comparison). Between orbits 1 and 6 (images 349673952 to 383758500), color observations show that the red ring broadened toward the west, covering some older bright deposits along its western margin, and darkened toward the south. The radii of the oval ring varied from 435 km in the east–west direction up to 650 km in the north–south direction, and its center was near 18° S, 255° W. Minor differences in the central dark deposits may have been caused by photometric variations, but similar changes can be seen even in closely matched color pairs. The minimum area covered by new deposits was $\sim 107,000$ km^2 but an area as large as 1,014,000 km^2 could have been affected by the change, if the entire ring and its interior are included. The maximum range of the deposition was at least 490 km to the west (620 km if the darkening to the south is included). Between orbits 7 and 8 (images 389772007 to 394552545), violet images show that a new bright rim appeared around the west edge of the ring, perhaps formed from SO_2 that was vented from the plume but was unable to condense on the warm red deposits. This bright rim ranged up to 425 km from the plume source. The red ring appeared to darken in the north and its shape changed toward the north and the east. Bright deposits toward the south were also overprinted. The area affected was at least 516,000 km^2, not counting the area interior to the red ring.

Pele was clearly active during Pillan's eruption, as shown by the changes that occurred between orbits 8 and 10 (images 394552445 to 413744179). Interference between the plumes of Pele and Pillan is demonstrated by the flattening of the boundary between the two distinct plume deposits. Color images (Plate 1E) show an enlarged bright deposit to the west, along the outside margin of the red ring, up to a maximum range of ~ 530 km from the source. The red ring enlarged and darkened toward the south, particularly in the southeastern area around the "notch" (the gap in Pele's ring that was evident in Voyager 1 images but filled in by the arrival of Voyager 2 (McEwen, 1988)). The central portion of the ring brightened, and violet filter images show that the

brightening was caused by the deposition of a large, quasi-circular deposit interior to the red ring. This new bright ring had a radius of 395 ± 30 km. All together, the area covered by new deposits was 626,000 km^2.

The ring's bright rim along its western exterior margin disappeared between orbits 10 and 11 (images 413744204 to 420833023), but in this case it seems likely that the SO_2 sublimated or was otherwise eroded instead of being buried by new red deposits. Pele continued to deposit red materials, as shown by the partial burial of the black Pillan ash to the northeast, and the red ring darkened toward the east and south. The apparent brightening of the central area was probably a photometric effect of the higher phase orbit 11 observations. The area covered by new deposits, assuming that the deposition at Pillan was experienced uniformly around the ring, was at least 894,000 km^2.

The overall shape of Pele's deposits changed subtly between orbits 11 and 21 (images 420833023 to 506484107), particularly in the violet filter. A new irregular dark deposit appeared around the central black materials at the ring center, out to a maximum distance of 160 km. Beyond this deposit, a new irregular bright ring was emplaced between the center and the red ring with a radius that varied from 280 to 330 km. The outer red deposits darkened and grew larger (maximum distance 580 km). Additionally, new bright deposits appeared along the outside margin of the red ring, toward the southwest. The area resurfaced was ∼ 697,000 km^2.

Obvious, large-scale changes to Pele's red ring took place between orbits 21 and 24 (images 506501107 to 520873452). The ring darkened, circularized, enlarged toward the north and east, and encroached further upon Pillan's dark deposit. The biggest ring shape changes took place to the south, where red deposits buried a bright SO_2 deposit at 37° S, 245° W, 720 km distant from the source (unless this was caused by another, unknown volcano). The total area changed was 1,009,000 km^2.

Bright materials (presumably SO_2 entrained in Pele's plume) were deposited in the middle of Pele's red ring between orbits 24 and 29 (images 520873426 to 584396885). The radii of this bright, oval ring were ∼ 340 km in the east–west direction and ∼ 530 km in the north–south direction. New red deposits were emplaced at the ring margin in the south and also to the northeast, where they continued to cover Pillan. The area changed was 616,000 km^2, excluding the (apparently unchanged) central zone inside the red ring.

Further minor modifications took place during the last imaging interval, between orbits 29 and 32 (images 584396885 to 625700552). The earlier white oval was buried or eroded and the ring darkened overall, filled an area of its perimeter in the southeast near the "notch", and enlarged toward the west. A new bright deposit appeared along the exterior margin in the west and southwest, reaching a maximum range of 580 km. The area affected (not counting the ring center) was ∼ 671,000 km^2.

3.18. Dazhbog

3.18.1. Description

Dazhbog (54° N, 302° W) is another volcano in the class of those that produced episodic, violent polar eruptions late in the Galileo mission. Although poorly imaged, Dazhbog's eruption produced an orange ring with dimensions that rival those of Pele. Thermal emission from Dazhbog was detected in HST NICMOS (Goguen et al., 1998) and PPR (Rathbun et al., 2003) observations, but no plume has been spotted there and the volcano was apparently inactive during the Voyager encounters. The highest resolution image of the area shows a large, near-circular patera ∼ 110 km in diameter and a small concentric ring.

3.18.2. Surface changes

Like Pillan, Dazhbog gave notice that it was about to erupt when the caldera darkened between orbits 6 and 24 (images 389772000 and 520873426), an event that may have taken place as early as orbit 21. Such events are common on Io (see Section 4), along with patera brightenings and color changes, and may signify transient heating within a caldera. Dazhbog's eruption took place between orbits 29 and 31 (images 584396885 to 615693245; Fig. 18) and produced a near-circular, bright central ring of radius 270 ± 25 km, centered at 55° N, 300° W. Color images (Plate 1H) show that a much larger, elongated orange ring was deposited outside the bright deposits, with a north–south radius of 480 km and an east–west radius of 370 km. Although the orbit 31 image has low resolution, it appears that the area immediately surrounding the caldera was stained with dark (presumably silicate) pyroclasts. The total area coated by the eruption was ∼ 582,000 km^2.

3.19. Ra

3.19.1. Description

Because of its colorful Voyager-era flows, Ra Patera (9S325) was considered a leading candidate for sulfur volcanism on Io (Pieri et al., 1984). Ra was the site of dramatic Voyager-to-Galileo surface changes (McEwen et al., 1998a) that began prior to the start of the Galileo mission: activity at Ra was indicated by HST observations during the interval between March, 1994 and July, 1995 (Spencer et al., 1997b). A small (∼ 75 km high) plume was seen over the region during orbit 1 but definitive nondetections were made during orbits 3 and 4, although an auroral glow was seen during orbit 4 (McEwen et al., 1998a). No thermal emission was detected by NIMS at any time during the mission, but NIMS had very poor spatial resolution over this region and the area was not observed during the period when the plume sighting was made (Lopes-Gautier et al., 1997; Lopes et al., 2001). Ra brightens conspicuously at high phase angles, suggesting a coating of forward-scattering frosts (Geissler et al., 2001b), and has even been observed during eclipse at a high phase angle while illuminated by

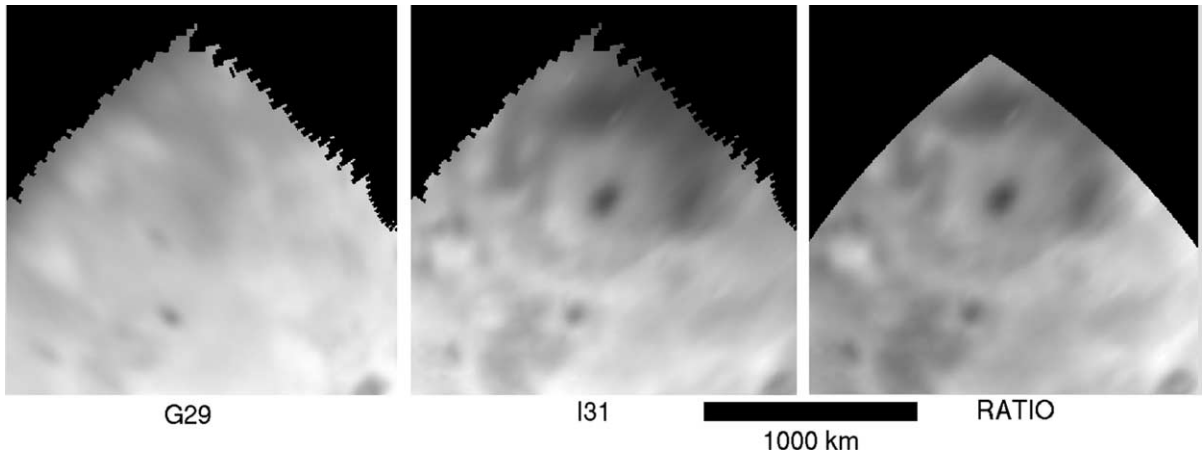

Fig. 18. Surface changes at Dazhbog: green filter images. The darkening of the central patera and emplacement of the giant ring are apparent even in these low resolution images. See also Fig. 21 and color Plate 1, part H.

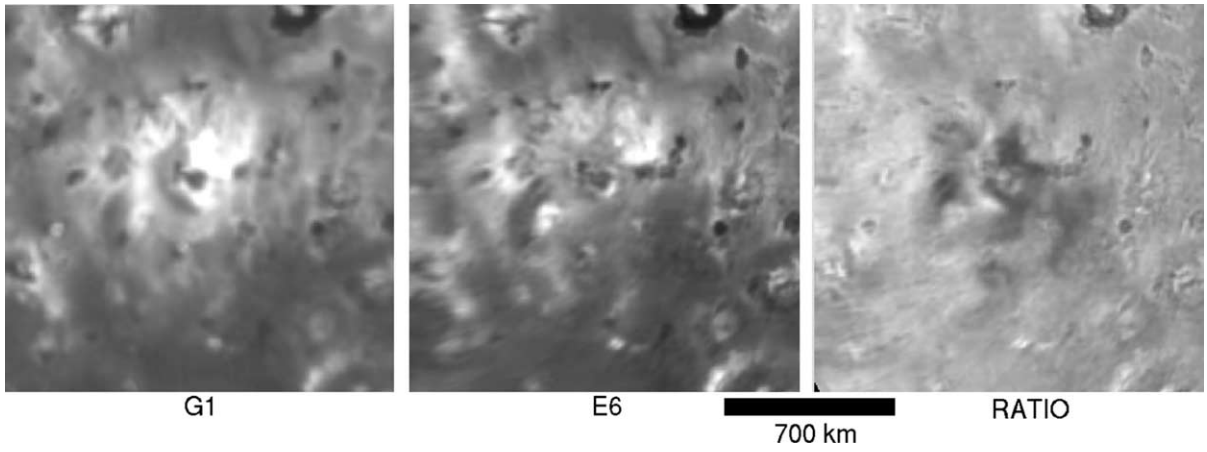

Fig. 19. Surface changes at Ra: violet filter images. New yellow deposits emplaced between orbits G1 and E6 appear dark in this filter.

sunlight that was faintly reflected from Jupiter (McEwen et al., 1998a).

3.19.2. Surface change

Despite the photometric variability of the region, it is clear that at least one eruption took place in the interval between orbits 1 and 6 (images 349746326 to 383758507; Fig. 19). New irregular yellow deposits were emplaced around an area centered at 10° S, 323° W that are conspicuously darker in the violet filter orbit 6 image (14° phase) than in the image from orbit 1 (25° phase). The maximum range of the deposition was 260 km, and the area changed was approximately 170,000 km^2.

3.20. Acala

3.20.1. Description

Acala Fluctus (11° N, 337° W) is the source of a curious plume that was often sighted by SSI in eclipse but never seen in daylight. Auroral glows were observed over Acala during orbits 7, 8, 9, 10, 11, and 15 but no dust-rich plumes were detected during favorable opportunities in orbits 1 and 10 (McEwen et al., 1998a; Geissler et al., 2001a). It was therefore a leading candidate for a gas-rich, dust-free "stealth" plume as predicted by Johnson et al. (1995). High-resolution images of the region, taken by Voyager 1, show a series of dark lava flows from a linear fissure-like system. Acala was a Voyager-era hot spot, and high temperature thermal emission was detected by SSI on orbits 9, 14, 15, and 21 (McEwen et al., 1998a; Keszthelyi et al., 2001). Acala was also detected in HST-NICMOS and ground-based thermal observations in 1997/1998 (Lopes et al., 2003). No surface changes could be distinguished at Acala up to orbit 10 (McEwen et al., 1998a), perhaps because of photometric variations complicated by the presence of forward-scattering frosts in this region (Geissler et al., 2001b).

3.20.2. Surface changes

Although it was never caught in the act, surface changes around Acala indicate that its stealthy plume must have deposited dust around the region on at least two separate occasions. Bright deposits were emplaced around a new dark spot (presumably a lava flow) between orbits 6 and 11 (images 383758507 to 420626404). Green filter images show

that an older dark spot at 7.8° N, 333.4° W disappeared during this interval and a new dark spot roughly 32 × 65 km in size appeared at 10.2° N, 332.1° W, 100 km to northeast. The disappearance was due to a blanket of bright materials that extended over the dark flows to the west across a distance up to 245 km. Violet images show that an irregular bright rim was emplaced around the fluctus on the west, south and east sides while new dark deposits were emplaced to the north, covering a total area of 142,000 km^2. These deposits were centered to the west of the new dark spot, near 10° N, 335° W, and reached a maximum range of 240 km (bright deposits) to 260 km (dark deposits). Careful re-examination of the green filter orbit 10 image (413791545) suggests that the new dark spot likely formed before orbit 10.

A second eruption took place between orbits 15 and 21 (images 450110968 to 506572423). A quasicircular bright ring was deposited to the northeast of Acala, centered near 12° N, 331° W. The approximate radius of the ring was 140 ± 10 km, but new deposits formed toward the northwest as far away as 250 km from the ring center, perhaps indicating two distinct eruptions. The area covered by new deposits was ∼ 150,000 km^2. These bright materials subsequently faded between orbits 21 and 31.

A useful "reality check" is provided by comparing well-matched green and violet filter images from orbits 6 and 22 (Fig. 20), all acquired near 14° phase. The comparison supports the above interpretations and confirms that Acala's plume sometimes lofted dust over the surrounding terrain, at least for brief periods.

3.21. Surt

3.21.1. Description

Surt (46° N, 338° W) was the site of a large-scale, episodic eruption between the encounters of Voyagers 1 and 2 that helped give rise to the notion that large Pele-type plumes constituted a class of eruptions, rather than an isolated occurrence (McEwen and Soderblom, 1983). By the time of Galileo's arrival, all traces of an eruption at Surt had vanished and the region had reverted to its Voyager 1 appearance. Thermal emission from Surt was detected by ground-based and HST observations early in the Galileo era (Spencer et al., 1997a; Goguen et al., 1998) and an extremely powerful outburst was detected during February, 2001 in adaptive optics observations by Marchis et al. (2002).

3.21.2. Surface change

Three lines of evidence suggest a major eruption near Surt late in the Galileo mission, between orbits 22 and 31 (images 512336700 to 615693245). First, new red deposits are clearly seen near 46° N, 334° W in the low resolution orbit 31 image that are not present in the sharper images from

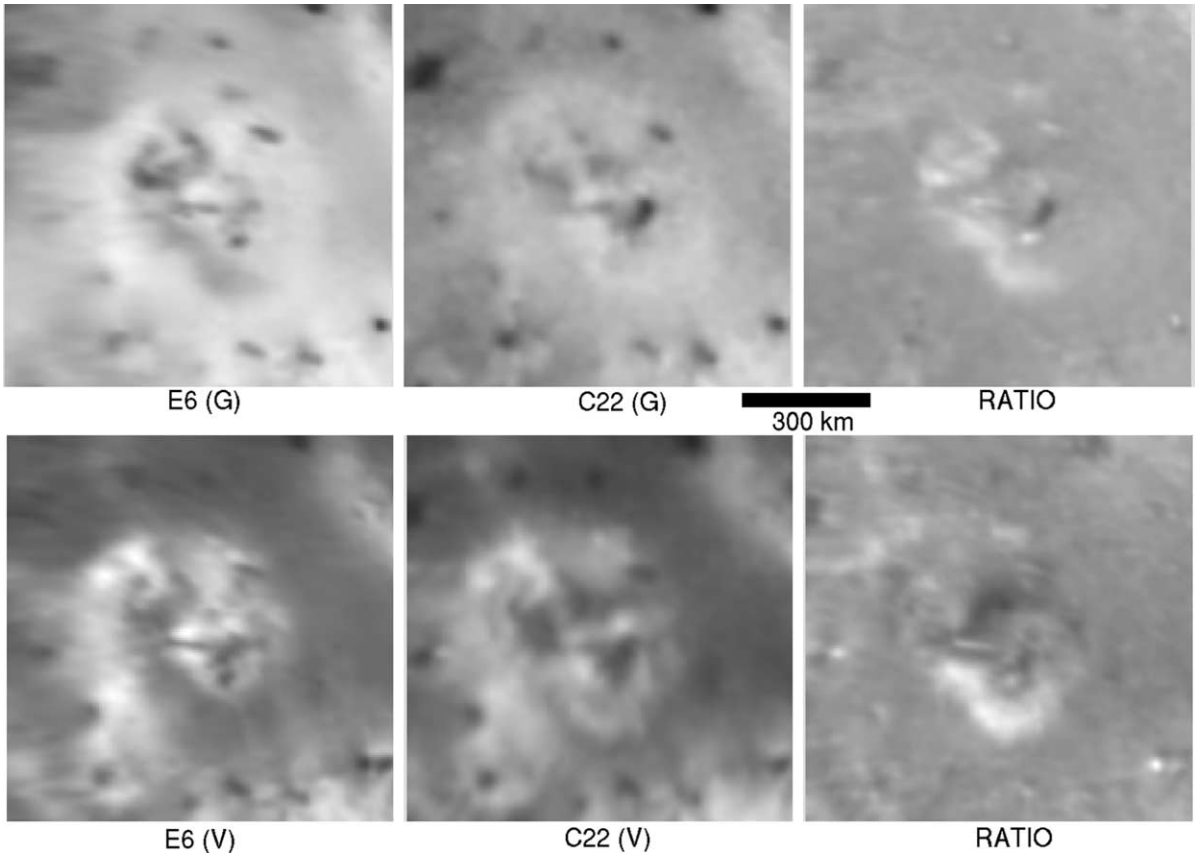

Fig. 20. Surface changes at Acala: green (G) and violet (V) filter images. The green filter images (top) show changes in the distribution or albedo of dark silicates, perhaps caused by the eruption of a new lava flow. The violet filter images (bottom) show the emplacement of new bright and dark plume deposits.

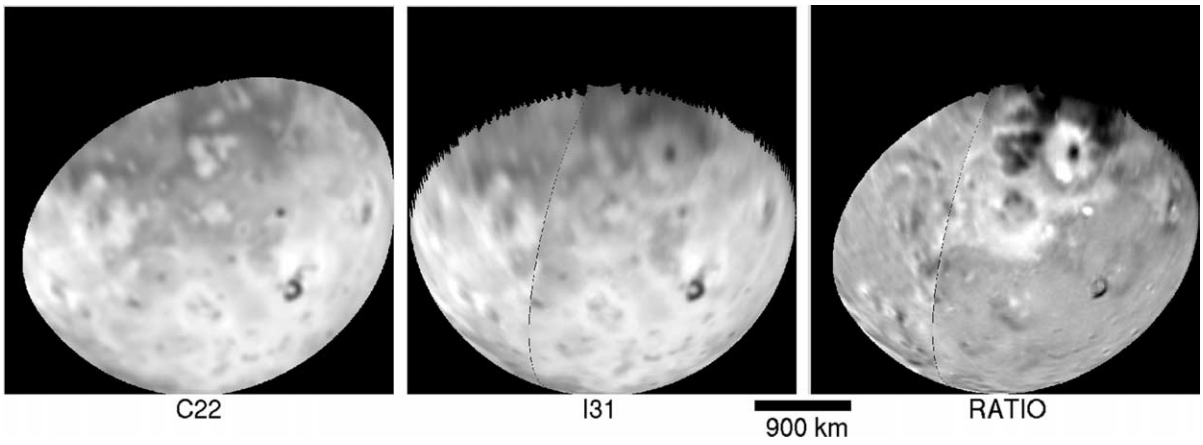

Fig. 21. Surface changes at Surt: green filter images. Surt is near the center of the picture. Its surface changes were much more subtle than those of nearby Dazhbog, above and to the right. See also color Plate 1, part H.

orbit 22 or earlier. Second, a nearly circular bright patch surrounds an area centered at 42° N, 335° W that is not apparent in the orbit 22 image despite closely matching phase angles (∼ 4°). It is best seen in a ratio of the two green filter images (Fig. 21). No such brightening is evident in the violet filter pictures, but neither is the prominent ring of nearby Dazhbog, perhaps because both of the deposits were orange to red in color (see Plate 1H). Third, a dark patera at 36° N, 321° W appears to have been buried by the eruption. Although small features can be difficult to discern in low resolution images, this feature can still be seen even when the orbit 22 image is blurred to the resolution of the later picture. The fact that it disappeared by orbit 31 suggests that it may have been buried by younger deposits. Our interpretation, albeit uncertain, is that a large orange ring with a radius of 380–390 km, centered near 42° N, 335° W, was deposited during an eruption that may have coincided with the ground-based sighting of a hot spot in the area during February, 2001 (six months prior to the orbit 31 imaging). This ring probably faded to some extent before it was imaged, and was partially overprinted by the eruption of Dazhbog. The area covered by the deposit may have been as much as 471,000 km^2. If so, this places Surt in a class of large-scale episodic eruptions that occurred near the north pole of Io during the Galileo era, along with Tvashtar, Dazhbog, "Thor," and the "North Polar Ring."

3.21.3. Other possibilities

Because of photometric variations, the limited temporal coverage and spatial resolution of the global monitoring data, and the transient nature of some plume deposits, several other possible large-scale surface changes may have taken place during the Galileo mission but were not positively identified by this survey. Suspected explosive eruptions may have taken place at Lei-Zi, Babbar, and an unidentified site south of Pele. Phillips (2000) describes a faint ring around Lei-Zi (15° N, 45° W) that was made apparent by dividing an orbit 9 violet filter image (401785407) by an earlier violet image from orbit 6 (383563726). The ∼ 190 km radius ring does not appear to change shape between the observations, so it could be a relic from an earlier eruption. Equally mysterious is the "notch" area southeast of Pele, which displays frequent brightness and color variations that are generally attributed to Pele but often appear independent of changes elsewhere in the red ring. Notable among these is the already-mentioned burial of bright SO_2 deposits at 37° S, 245° W, 720 km distant from Pele, between orbits 11 and 21 (images 420833023 to 506484107). Irregularities in Pele's ring toward the south and southeast of Pele have been explained as partial obstructions and clearings of Pele's vent (e.g., McEwen et al., 1998a), but it is possible that an as yet unidentified volcanic center was active in this region.

Babbar (38° S, 272° W) is another eruptive center that is difficult to characterize in terms of activity, in this case because of pronounced photometric variations associated with its dark pyroclastic deposits. Between orbits 8 and 10 (Plate 1E), Babbar appeared to change shape and brighten, depositing a bright ring 125 km in radius that was centered at 40° S, 72° W and covered an area of 50,000 km^2. Photometric variations appear inadequate to explain the change, because both images (394552600 to 413744204) were acquired at relatively high phase angles (73° and 61°).

4. Small scale changes and nonchanges

4.1. Patera color and albedo changes

In Section 3, we mentioned several examples of volcanic centers such Pillan, Kaminari and Dazhbog that gave notice of impending eruptions by changing color or albedo prior to producing plumes or notable surface changes. Many other paterae were observed to darken or brighten during the Galileo mission. We assume that these changes were caused by thermal activity that either heated the surfaces of the paterae (causing existing SO_2 to sublimate away), heated the SO_2 surrounding the paterae (liquifying the ice so that it could flood and brighten the paterae interiors), or produced

eruptions of fresh lava that darkened the surfaces of the paterae.

Gish Bar (17° N, 90° W) is one of the paterae that altered in appearance between observations taken during orbits 21, 24, and 32 (images 506406626, 520798504, and 625599500) (Perry et al., 2003). First, the eastern edge of the patera darkened in the 4 months between orbits 21 and 24, likely indicating an eruption of new lavas within the patera. By the time it was seen again at high resolution two years later, the west side of the patera had darkened, affecting an area of less than ~ 6000 km^2. This change was only apparent because of the availability of high-resolution ($\sim$ 250 m/pixel) imaging observations, suggesting that many more such small differences might be detected if similar high-resolution coverage were available for other paterae. Even given the limitations of the global-monitoring data, a half-dozen other instances of patera brightness and color variations were detected. Itzamna (16° S, 99° W) darkened on its west side, changing the shape of the patera and possibly producing dark pyroclastic deposits between orbits 6 and 7 (images 383600826 to 389654026), affecting an area of ~ 2000 km^2. Camaxtli (14° N, 136° W) darkened with no change to the nearby dark ash deposits between orbits 14 and 21 (images 440873539 to 506406626), altering an area less than 1800 km^2. Camaxtli was first detected by NIMS during orbit 15, although the region had previously been observed several times at similar spatial resolutions. Shamash (32° S, 152° W) brightened and turned green while the volcano deposited new bright SO_2 deposits toward the south that are visible in comparisons of color images taken during orbits 2 and 21. Violet filter images indicate that the eruption likely took place between orbits 11 and 14 (images 420743485 to 440873652), depositing bright materials to a maximum range of 167 km that covered an area of 22,000 km^2. Close to Pillan, Reiden (13° S, 234° W) indicated its activity by erupting through the dark ash deposited by Pillan shortly after the latter's eruption (orbit 10, image 413744204). A small white ring appeared around Reiden by orbit 21 (image 506492200) and new red deposits were visible to the east of Reiden by orbit 24 (image 520873426). Amaterasu (38° N, 307° W) darkened noticeably between orbits 1 and 6 (images 349746326 to 383758507) but failed to produce a subsequent eruption. An unnamed patera north of Mazda (at 6° S, 311° W) flickered briefly, brightening between orbits 6 and 10 (images 383758500 to 413791545) and then turning black again between orbits 10 and 15 (images 413791545 to 450110900).

Other possibilities include an unnamed patera at 47° S, 118° W that appeared to darken during orbit 21, perhaps as a result of better spatial resolution, and two paterae (Haokah, 21° S, 185° W and Mulungu, 17° N, 218° W) that appeared brighter in high-phase-angle images taken during orbits 8, 9, and 11 than in lower-phase images taken earlier or afterward. Haokah was detected as a hot spot by NIMS in orbits 11 and 14, while thermal emission from Mulungu was detected many times by NIMS throughout the Galileo Mission (R. Lopes, personal communication, 2003).

4.2. High-resolution changes

Two areas, Prometheus and Amirani, were imaged at high resolution during both orbits 24 and 27. The results of these experiments were described in detail by McEwen et al. (2000) and Keszthelyi et al. (2001), whose conclusions are summarized here for completeness. Repeated imaging of Amirani showed that new lavas covered an area of ~ 620 km^2 during the 134-day interval between the observations, erupting at rates estimated to be in the range 50 to 500 m^3/s. The lavas erupted from 23 separate breakouts scattered across the flow field, generally appearing as extensions of dark patches that were already visible in the orbit 24 image. These recent flows were hot enough to be detected by NIMS infrared observations (Lopes et al., 2001) and presumably too warm or too fresh to have been buried by plume fallout. A similar distribution of new lava flows was seen at Prometheus, covering a total of ~ 60 km^2 over the same time period. The new flows appeared at several locations at the distal end of the flow field, near the center of the bright ring. These observations suggested to Kieffer et al. (2000) that Prometheus' dusty plume is generated by the vaporization of SO_2 ices heated by the silicate lavas overlying the volatiles. In addition, new bright streaks formed at the margin of the flow field, suggesting that small plumes were produced as the hot lava encroached on the surrounding ices (Milazzo et al., 2001).

The occurrence of new lava flows at numerous locations within the Amirani and Prometheus flow fields is consistent with their interpretation as compound inflated pahoehoe, formed by a repetitive process in which lava is injected beneath an insulating crust and thickens the flow until it breaks out to form a new lobe. This mechanism helps explain the great lengths of the lava flows (up to 300 km in the case of Amirani, the longest active flow in the Solar System).

4.3. Specular reflection at Loki

Not really a surface change, but still worthy of mention, is a brief flash of light from the surface of Loki Patera (13° N, 309° W) during the orbit 21 plume movie sequence. The southern portion of Loki's dark surface brightened noticeably in image 506550623 when compared to the images taken just beforehand and just afterward. Because the incidence angle and the emission angle at Loki were nearly equal at the time that this image was taken, we interpret this brightening as a result of specular reflection from the dark flows on Loki's surface. The reflection was rather diffuse: the subsolar latitude was 2.8° when the sun glint was seen, so subtracting that from Loki's latitude yields at least $\sim 10°$ for the angular extent of the reflection. This observation suggests that Loki's lavas had a surface that was either glassy or extraordinarily smooth, consistent with its bright appearance

in a later high phase angle image from orbit 32. A similar diffuse glint was observed from Mazda Patera (9° S, 314° W) during the Voyager 1 flyby.

5. Discussion

5.1. Classes of surface changes

The surface changes noted above divide into three main categories: volcanic plume deposits, patera color or albedo changes, and seepages of SO_2. Episodic brightenings interpreted to be caused by SO_2 seepages were detected at Haemus Montes, Zal Montes, Dorian Montes, and the plateau to the north of Pillan Patera. All of these are regions with pronounced topography adjacent to active volcanic centers. These topographic variations, coupled with the photometric properties of SO_2 frosts, complicate the identification of genuine surface changes in such areas. However, we note that many mountain massifs on Io are surrounded by bright haloes of SO_2; such deposits must be frequently refreshed to remain visible on Io, where volcanic resurfacing and erosion or alteration efficiently erase thin surficial markings. We suggest that Galileo observed the regeneration of SO_2 frosts along the bases of mountain ranges at these four locations, perhaps triggered by volcanic heating of frozen ices caused by activity at nearby volcanic centers.

Smaller-scale changes in color or albedo that were localized to patera surfaces were found at Gish Bar, Itzamna, Camaxtli, Kaminari, Reiden, Pillan, Dazhbog, Amaterasu, and an unnamed patera north of Mazda. Except for Kaminari and the unnamed patera, all of these are recognized hot spots. In some cases (Pillan, Kaminari and Dazhbog), the paterae later produced a major eruption that altered the surrounding surfaces for hundreds of kilometers in extent. In other cases, the changes probably signified local heating that was restricted to the paterae. No visible signs of surface changes larger than a few tens of km in extent were seen at many volcanic centers known to be actively erupting during the period of Galileo imaging observations. The most flagrant case is Loki, which experienced several episodes of dramatic brightening at infrared wavelengths including a major event in mid-1999 in which Loki's 3.4 μ brightness increased by an order of magnitude (Howell et al., 2001). The most likely explanation for these stealthy eruptions is the eruption of lava onto surfaces that are already lava-covered, for example by the overturning of lava lakes (e.g., Rathbun et al., 2003).

Several distinctions can be made between classes of volcanic plume deposits on Io. Some deposits such as that from Ra's early eruption are irregular in plan, perhaps because of vent geometry or lack of sustained activity, while other volcanoes such as Prometheus produced clearly defined rings from long-lived, umbrella-shaped plumes. Most of the surface changes observed by Galileo displayed both characteristics, producing complete or partial rings as well as additional deposits within or exterior to the rings. A more fundamental classification is according to the size of the deposits, such as the radii of the rings (where visible) or the maximum ranges of irregular deposits. Figure 22 shows the number of plume-deposit rings observed as a function of their radius; here we have counted only those rings with distinct center coordinates, so for example Masubi is counted twice (because the ring center shifted location between eruptions) whereas Pele is counted only once, although it erupted several times. The modal radius is between 150 and 200 km, and more than half of the 22 distinct rings observed have radii between 150 and 250 km. In contrast, only six rings have radii greater than 350 km: unnamed (south of Karei), the North Polar Ring, Tvashtar, Pele, Dazhbog and Surt. All of these giant rings are orange or red (rather than the white or gray colors of the smaller rings) and all of the well-imaged giant rings are oval rather than circular, with radii in the north–south direction significantly larger than their radii in the east–west direction. For this chart we have chosen the mean of the north–south and east–west radii to represent the size of the giant rings, and chosen the largest radius to represent the size of the smaller circular rings that erupted on several occasions from the same location.

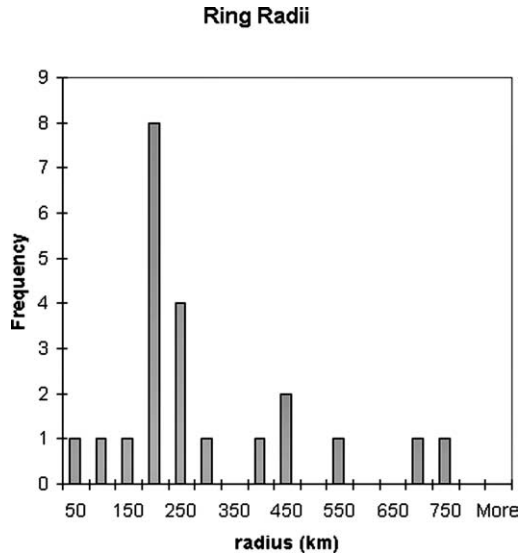

Fig. 22. Histogram of radii of plume deposit rings.

The distinction between small and large plumes is made even clearer when the maximum extents are plotted for all surface changes, whether or not they produced a clearly defined ring, and for all eruptions (including repeated eruptions from the same volcanic center). Figure 23 shows that the deposits emplaced by all of the large scale explosive eruptions fall into two categories with two distinct distributions. The majority of eruptions deposited materials that reached distances between 50 and 350 km, peaking at ranges between 150 and 200 km. A much smaller class of giant eruptions deposited materials as far as 350–800 km, with a broad distribution that peaked at maximum distances of 500–550 km from the eruptive centers. These observations (coupled with the fact that the giant ring deposits tend to be red or orange)

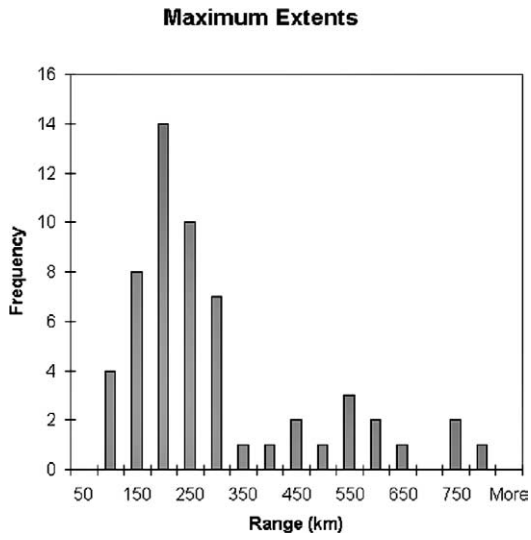

Fig. 23. Histogram of maximum ranges of all plume deposits.

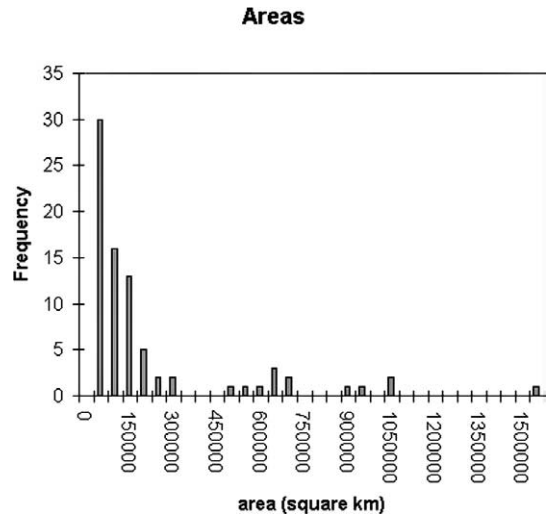

Fig. 24. Histogram of areas covered by plume deposits.

support the suggestion of McEwen and Soderblom (1983) that there are two classes of plumes on Io that are driven by different volatiles. The smaller plume deposits are produced by the explosive volatilization of SO_2; entrainment of silicate ash or sulfur compounds may cause discoloration of the resulting plume deposits, as was the case for Pillan. The larger plumes must contain significant quantities of sulfur in order to produce extensive red or orange deposits; an S_2:SO_2 mixing ratio of 0.1 was determined for Pele's plume by HST measurements (Spencer et al., 2000).

The areas resurfaced during explosive eruptions are of course dominated by the largest events. A plot of the number of surface changes vs. the areas coated by new materials (Fig. 24) shows a steeply declining distribution that peaks between 50,000 and 100,000 km^2 and tapers off at larger areas, with the maximum area covered in a single eruption being that of Tvashtar.

5.2. *Locations of surface changes*

Much of Io remained unaltered over the course of the Galileo mission, while some areas were resurfaced repeatedly. Figure 25 shows the areas that were determined to have been covered by new volcanic plume deposits, summed so that the brightness of each area is determined by the frequency of resurfacing over the 5-year period of imaging observations. Unfortunately we have no way of determining the depth of deposition of the pyroclastic deposits, nor does the plot take into account the erasure of plume deposits such as was observed at Kanehekili, Masubi, Zamama, Acala and probably the large ring surrounding the unnamed patera south of Karei. However, Fig. 25 gives the correct qualitative impression that multiple eruptions took place at several locations including Kanehekili, Prometheus, Culann, Zamama, Marduk, and particularly Pele which was seen to alter 8 times over the course of the Galileo mission. Because of its great size and sustained activity, Pele by itself accounts for 40% of the total resurfacing by plume deposits (adding together each of Pele's separate eruptions), more than 4 times the area covered by the largest singular eruption at Tvashtar. On the other hand, approximately 83% of Io's surface never visibly altered over the entire Galileo era.

Nearly all of the bright plume deposits are associated with thin frosts of fine-grained SO_2 that are visible at high phase angles, whereas none of the six giant rings produced such frost deposits. Most of Io's equatorial region is dominated by a band of high-albedo ice that appears relatively bright at low phase angles but becomes darker than the poles when Io is seen at higher phase. NIMS spectral measurements (Carlson et al., 1997) suggest that this strongly backscattering equatorial band is made up of relatively coarse-grained SO_2. Disk-resolved photometric analysis (Geissler et al., 2001b) revealed many localized patches within the equatorial zone that are transparent at low phase angles but appear prominently bright at high phase. From NIMS compositional maps, many of these patches were found to correspond to local deposits of SO_2 that were presumably derived from volcanic activity (Doute et al., 2001, 2003, in preparation). They were interpreted as thin (< 1 cm) frosts of fine-grained (a few microns diameter) SO_2 that are isotropic- to slightly forward-scattering. Such frosts are not expected to survive long at low latitudes before they anneal into coarse-grained ices and crystal aggregates. Fine-grained frosts were identified at Masubi, Amirani, Arinna, Prometheus, Culann, Zamama, Marduk, Ra, and Acala: all sites of surface changes that were presumably produced by SO_2-rich plumes. Frosts were not clearly shown near Kanehekili but this region was poorly fit by the photometric model, presumably because of the frequent surface changes in the area. Many other low-latitude regions were identified as frost-rich, but displayed no surface changes during the period of Galileo observations: patches of frost were identified to the west of Karei at 4° N, 23° W, and at Surya, Mycenae Regio (near Nina Patera), Volund, Daedalus, and Loki. We speculate that these

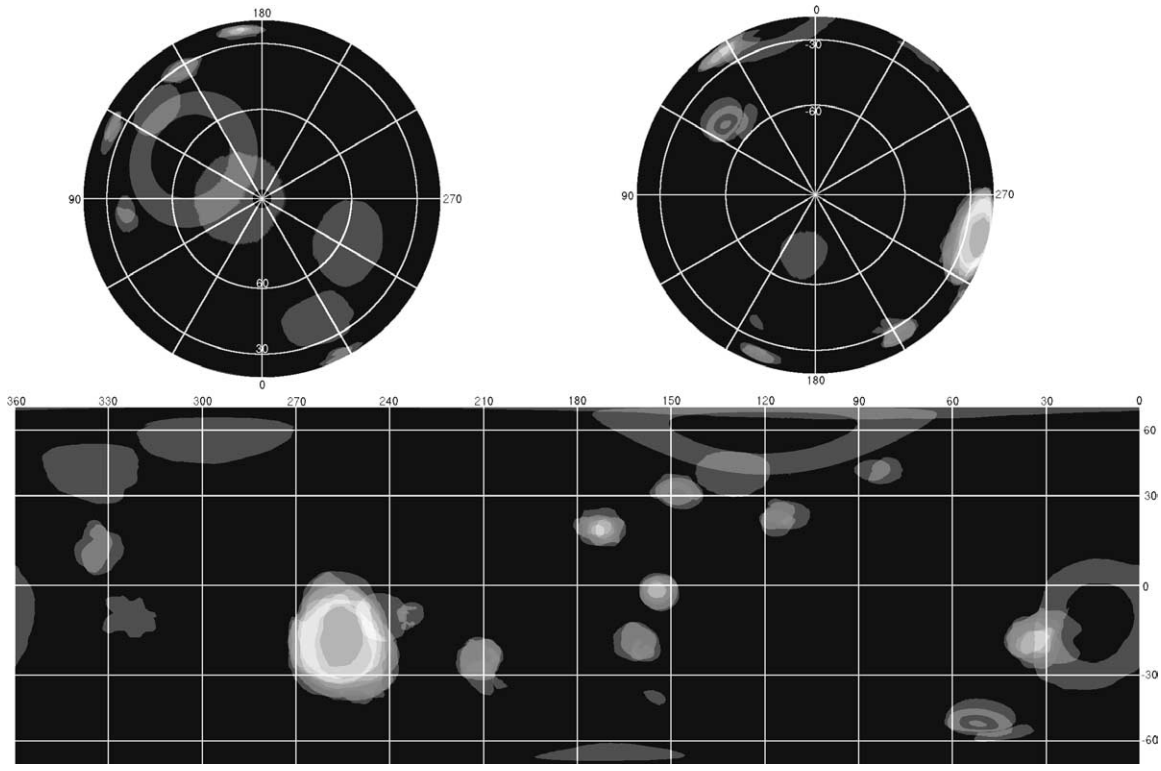

Fig. 25. Map of locations of resurfacing by plume deposits. The brightness represents the frequency of deposition rather than the thickness of the deposits.

areas may be sites of recent plume activity that was missed by Galileo; plumes at Volund and Loki were spotted by Voyager.

5.3. Eruption history

From observations of surface changes, plumes, and auroral emissions seen in Galileo SSI images, we can construct a timeline of major explosive eruptions over the past five years. Figure 26 shows what erupted when, to within (sometimes very loose) limits imposed by the imaging coverage. An encouraging sign is that the surface changes and plume detections agree—there are surface changes seen at the locations and dates of every plume detection, although of course there are many surface changes for which we missed seeing any plumes. Even Acala, which was not seen in sunlight, produced notable surface changes during unobserved periods when its plume must have entrained dust.

Little correlation can be seen between explosive eruptions and the appearance of most high-temperature hot spots. Fully three quarters of the high-temperature hot spots detected by SSI were unaccompanied by noticeable surface changes, perhaps suggesting that many of these eruptions resurfaced older lava or were confined to lava lakes. About half of the large-scale surface changes were in areas in which SSI failed to detect high temperature lavas, although most were detected from NIMS or ground-based observations at longer wavelengths. There is good agreement between sur-

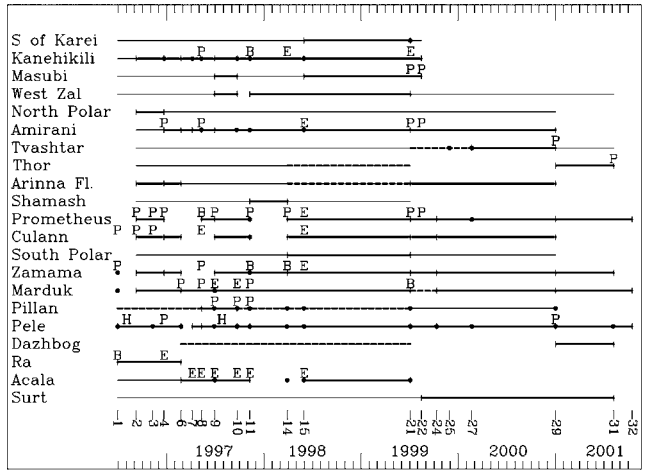

Fig. 26. Timeline of major eruptions. Observations of surface changes, plumes, and high-temperature hot spots are combined to show the chronology of Io's major explosive eruptions from 1996 to 2001. Observations were acquired only during the orbits listed at the bottom. For each volcanic center, a thick line bounded by vertical bars indicates an interval during which a large-scale surface change occurred. Dashed lines indicate lesser changes, such as darkening of a patera. A thin line indicates an interval over which there were no detectable changes. No lines are shown during periods when there was no imaging coverage or the image quality was too poor to tell. Sightings of plumes in sunlight are denoted with a P. Plumes identified by their auroral emission in eclipse are marked E, and plumes seen both in daylight and in eclipse are marked by B. Dots along the lines denote dates when high-temperature lavas were detected by SSI.

face changes and sightings of hot lava at Kanehekili, Zal, Camaxtli, Pillan, Pele, and Acala.

However, there may be a correspondence between extremely high temperatures and plumes. There are 4 well-documented eruptions with temperatures exceeding 1400 K: Pillan, Masubi (Goguen et al., 1998), Pele (Lopes et al., 2001), and Surt (Marchis et al., 2002). Tvashtar is also believed to have had such high temperatures, based on analysis of SSI near-infrared images (Milazzo 2003, this issue). Contemporaneous plumes were also observed at all of these locations except Surt, where surface changes suggest a plume eruption. Such high temperatures may indicate the presence of lava fountaining, which is driven by volatiles that may also produce large plumes in Io's extremely tenuous atmosphere.

As expected, explosive volcanism on Io was sporadic in timing. Plume activity at various volcanic centers ranged from intermittent to continuous. Polar eruptions (Surt, Dazhbog, Tvashtar, N. Polar Ring, S. Polar Ring) tended to be episodic: a singular eruption preceded or followed by a long period of quiescence. Equatorial eruptions were usually more persistent and smaller. Pele seemed to be continuously active, with the possible exception of the period between orbits 6 and 7. Apart from Pele, the largest eruptions took place prior to orbits 4 (N. Polar Ring), 21 (S. of Karei), 29 (Tvashtar), and 31 (Thor, Dazhbog, and Surt).

5.4. Implications

Perhaps the most surprising result of this survey is the small number of volcanic centers that visibly altered their surroundings: out of more than a hundred active volcanoes identified by their thermal signature (Lopes et al., 2001) and over 450 paterae that are geologically youthful and considered potentially active (Radebaugh et al., 2001), only 28 produced noticeable surface changes more than a few tens of km in extent over the past five years. Few of the high temperature thermal events detected by SSI were accompanied by plume activity, and even the powerful upheavals of Loki left no mark on the surrounding landscape. Apparently, most of Io's heat loss must take place by the resurfacing of existing lavas, for example in lava lakes, rather than the eruption of new flows onto volatile-rich surfaces.

On the other hand, it seems likely that plume deposits could contribute substantially to the resurfacing needed to bury impact craters on Io, estimated at 1 mm/year averaged globally (Spencer and Schneider, 1996). An area equivalent to only 17% of Io's surface was covered by plume deposits over the five year Galileo period, requiring an average plume deposit thickness of ~ 3 cm (accumulated over 5 years) in order to account for crater burial. Given that 2/3 of this area was covered by red and orange deposits that could be much thinner, the SO_2-rich plumes are required to accumulate deposits of several centimeters thickness over 5 years. Keszthelyi et al. (2001) argue that this is plausible in the case of Pillan, provided that 10% of the estimated silicate magma volume was converted to pyroclastics. Applying the same assumptions to Amirani and Prometheus yields plume deposit accumulations of ~ 1 cm and ~ 0.1 cm respectively, if the lava effusion rates observed between orbits 24 and 27 remained constant over the full five years. These are lower limits, obtained by considering only the silicates in the plume deposits. Plume deposits are likely to be much thicker because of the volatilization of ices by hot lava. Indeed, the surface changes surrounding Prometheus indicate substantial plume deposit thicknesses in order to be apparent at visible wavelengths, where SO_2 is quite transparent. Estimates based on the optical thickness of Prometheus' plume (e.g., James and Wilson, 1998) suggest that dust accumulations of at least 2 cm per year are likely. Similar estimates applied to giant plumes such as Pele (Lee and Thomas, 1980; Spencer et al., 2000) yield much smaller accumulation rates, on the order of 0.1 mm/year, owing to their low optical thicknesses and small particle sizes.

Fading of surface changes on time scales of months to years was observed at several locations including Kanehekili, Masubi, Zamama, Acala and probably the large ring surrounding the unnamed patera south of Karei. The mechanisms of erasure may have included thermal metamorphism (from fine-grained frosts to coarse grained ices and crystal aggregates) and chemical alteration (from red short-chain sulfur allotropes to more stable yellow S_8). Erosion due to charged particle sputtering (at a rate of less than 1 μm per year; Haff et al., 1981) is unlikely to have been effective over such short time scales. In addition, burial of older pyroclastics by new volcanic plume deposits was particularly apparent at Pillan (by Pele and Kaminari) and Tvashtar (by Thor). Such erasure may account for the discrepancy between the number of surface changes noted in Voyager to early Galileo image comparisons (~ 30 over 20 years; McEwen et al., 1998a) and the number of distinct sites of change noted in this survey (also 30, but over a period of only 5 years).

Although the giant plumes contribute little to the resurfacing of Io, they probably dominate the escape of dust from the satellite into the jovian space environment because of their higher dust ejection velocities. Galileo Dust Detector measurements indicated orbit-to-orbit variations of up to three orders of magnitude in the quantity of dust near Jupiter (Krueger et al., 2002) that could be attributed to Io through periodic variations linked to Io's orbit (Graps et al., 2000). Although much of this variation was likely due to Pele, it is instructive to compare the Dust Detector measurements with the record of giant episodic plumes on Io. Peaks in dust density occurred during orbits 4, 21, 29, and 30 (Krueger et al., 2002), coinciding with the appearance of the North Polar Ring (first seen on orbit 4), the giant ring South of Karei (orbit 21), Tvashtar (orbit 29) and the triad of Thor, Dazhbog and Surt (first detected on orbit 31, but no imaging observations of Io were made during orbit 30). Despite the fact that the giant plumes are tenuous, a simple calculation shows that they easily supply enough mass to account for the flux of dust escaping Io. All together, at least 10 million

square kilometers of Io's surface were covered by red and orange plume deposits, when repeated eruptions are added up over the course of the Galileo mission. Assuming that each eruption produced a coating only 10 μ thick (the minimum needed to be visible), and that the deposits have a density of 1500 kg m^{-3}, this suggests that at least 1.5×10^{11} kg of sulfur-rich solids were emplaced on Io's surface, or three orders of magnitude greater than the total mass of dust estimated to have escaped the satellite over the same time period (~ 1 kg s^{-1}; Krueger et al., 2002).

6. Conclusions

Based on repetitive Galileo SSI imaging, we have documented 82 apparent surface changes that took place on Io during the 5 year mission, determined as closely as possible the dates of the changes, and made measurements for each new deposit of the areal extent, maximum range, and radius of any ring present. Explosive volcanic activity was revealed at four previously unrecognized centers: an unnamed patera to the south of Karei that produced a Pele-sized red ring, a patera to the west of Zal that produced a small circular bright deposit, a large orange ring discovered near the north pole of Io, and a small bright ring near Io's south pole. From this survey we can draw the following conclusions:

1. A minority of Io's active volcanoes produce large scale surface changes. Most of the hot spots detected from SSI, NIMS and ground-based thermal observations caused no noticeable surface changes greater than 10 km in extent over the five year period of Galileo imaging observations. This indicates most of Io's heat loss must take place by the quiet resurfacing of existing lavas, for example in overturning lava lakes, rather than the eruption of new flows onto volatile-rich surfaces. On the other hand, surface changes always accompany plume activity, implying that no Ionian plumes are completely dust-free.
2. Two types of plumes are distinguished on the basis of the size and color of their deposits, confirming post-Voyager suggestions by McEwen and Soderblom (1983) that were based on a more limited data set. Measurements of both ring radii and maximum deposit extents show two distinct populations of plumes, presumably powered by different volatiles. Smaller plumes produce near-circular rings typically 150–200 km in radius that are white or yellow in color unless contaminated with silicates, and frequently coat their surroundings with frosts of fine-grained SO_2. The larger plumes are much less numerous, limited to a half dozen examples, and produce oval orange or red, sulfur-rich rings with maximum radii in the north–south direction that are typically in the range from 500 to 550 km. Both types of plumes can be either episodic or quasi-continuous over a five year period.
3. Substantial thicknesses are required in order for the SO_2-rich plume deposits to be apparent at visible wavelengths. Repeated eruptions of the smaller SO_2-rich plumes likely contribute significantly to Io's resurfacing rate, whereas dust ejection is likely dominated by the tenuous giant plumes. Both types of plume deposits fade on time-scales of months to years through burial and alteration, accounting for the discrepancy between the number of Galileo era surface changes and the number of Voyager-to-Galileo changes.
4. Surface changes and other image-to-image variations that are not directly attributable to volcanic plume deposits also yield information about volcanism on Io. Episodic seepages of SO_2 at Haemus Montes, Zal Montes, Dorian Montes, and the plateau to the north of Pillan Patera may have been triggered by activity at nearby volcanic centers. Specular reflection from the surface of Loki suggests that the surface of the lava lake is either extraordinarily smooth or else coated with a glassy rind.

Acknowledgments

We thank Mariam Totonchy, Jani Radebaugh, Jason Perry and Elizabeth Turtle for calling several surface changes to our attention. P.G. wishes to thank Gian Gabriele Ori and the staff of IRSPS for their hospitality while this paper was written. We also thank Rosaly M.C. Lopes and Lionel Wilson for constructive comments and corrections.

References

Carlson, R.W., Smythe, W.D., Lopes-Gautier, R.M.C., Davies, A.G., Kamp, W.L., Mosher, J.A., Soderblom, L.A., Leader, F.E., Mehlman, R., Clark, R.N., Fanale, F.P., 1997. Distribution of sulfur dioxide and other infrared absorbers on the surface of Io. Geophys. Res. Lett. 24, 2479–2483.

Cook, A.F., Shoemaker, E.M., Smith, B.A., Danielson, G.E., Johnson, T.V., Synnott, S.P., 1981. Volcanic origin of the eruptive plumes on Io. Science 211, 1419–1422.

Davies, A.G., McEwen, A.S., Lopes-Gautier, R.M.C., Keszthelyi, L., Carlson, W.R., Smythe, W.D., 1997. Temperature and area constraints of the South Volund Volcano on Io from the NIMS and SSI instruments during the Galileo G1 orbit. Geophys. Res. Lett. 24, 2447–2451.

Davies, A.G., Keszthelyi, L.P., Williams, D.A., Phillips, C.B., McEwen, A.S., Lopes, R.M.C., Smythe, W.D., Kamp, L.W., Soderblom, L.A., Carlson, R.W., 2001. Thermal signature, eruption style, and eruption evolution at Pele and Pillan on Io. J. Geophys. Res. 106, 33079–33104.

de Pater, I., Marchis, F., Macintosh, B., Roe, H.G., Le Mignant, D., Graham, J.R., Davies, A.G., 2004. Keck AO observations of Io in and out of eclipse. Icarus 169, 250–263.

Doute, S., Schmitt, B., Lopes-Gautier, R., Carlson, R., Soderblom, L., Shirley, J., The Galileo NIMS Team, 2001. Mapping SO_2 frost on Io by the modeling of NIMS hyperspectral images. Icarus 149, 107–132.

Frank, L.A., Paterson, W.R., 2001. Survey of thermal ions in the Io plasma torus with the Galileo spacecraft. J. Geophys. Res. 106, 6131–6150.

Geissler, P.E., McEwen, A.S., Ip, W., Belton, M.J.S., Johnson, T.V., Smyth, H.W., Ingersoll, A.P., 1999a. Galileo imaging of atmospheric emissions from Io. Science 285, 870–874.

Geissler, P.E., McEwen, A.S., Keszthelyi, L., Lopes-Gautier, R., Granahan, J., Simonelli, D.P., 1999b. Global color variations on Io. Icarus 140, 265–282.

Geissler, P.E., McEwen, A.S., Phillips, C., Keszthelyi, L., Turtle, E., Milazzo, M., Lopes-Gautier, R., Simonelli, D.P., Williams, D.A., Galileo Imaging Team, 2000. New results on Io's color and composition. In: Proc. Lunar Planet. Conf., p. 1968. Abstracts 31.

Geissler, P.E., Smyth, W.H., McEwen, A.S., Ip, W., Belton, M.J.S., Johnson, V.T., Ingersoll, A.P., Rages, K., Hubbard, W., Dessler, A.J., 2001a. Morphology and time variability of Io's visible aurora. J. Geophys. Res. 106, 26137–26146.

Geissler, P., McEwen, A., Phillips, C., Simonelli, D., Lopes, R.M.C., Doute, S., 2001b. Galileo imaging of SO_2 frosts on Io. J. Geophys. Res. 106, 33253–33266.

Goguen, J.D., Davies, A.G., 1999. Constraints on Io's high-temperature volcanism from HST NICMOS images. In: 1999 AGU Fall Meeting, San Francisco. Abstract P41B-02.

Goguen, J.D., Lubenow, A., Storrs, A., 1998. HST NICMOS images of Io in Jupiter's shadow. Bull. Am. Astron. Soc. 30, 1120.

Goguen, J.D., Matson, D.L., Sinton, W.M., Howell, R.R., Dyck, H.M., 1988. Io hot spots—infrared photometry of satellite occultations. Icarus 76, 465–484.

Graps, A.L., Grun, E., Svedhem, H., Kruger, H., Horanyi, M., Heck, A., Lammers, S., 2000. Io as a source of the jovian dust streams. Nature 405, 48–50.

Haff, P.K., Watson, C.C., Yung, Y.L., 1981. Sputter ejection of matter from Io. J. Geophys. Res. 86, 6933–6938.

Howell, R.R., 1997. Thermal emission from lava flows on Io. Icarus 127, 394–407.

Howell, R.R., Spencer, J.R., Goguen, J.D., Marchis, F., Prange, R., Fusco, T., Blaney, D.L., Veeder, G.J., Rathbun, J.A., Orton, G.S., Grocholski, A.J., Stansberry, J.A., Kanner, G.S., Hege, E.K., 2001. Ground-based observations of volcanism on Io in 1999 and early 2000. J. Geophys. Res. 106, 33129–33140.

James, M.R., Wilson, L., 1998. An optical model for ballistic plumes on Io. In: Proc. Lunar Planet. Conf., p. 1349. Abstract 29.

Johnson, T.V., Matson, D.L., Blaney, D.L., Veeder, G.J., Davies, A., 1995. Stealth plumes on Io. Geophys. Res. Lett. 22, 3293–3297.

Keszthelyi, L., McEwen, A.S., Phillips, C.B., Milazzo, M., Geissler, P., Turtle, E.P., Radebaugh, J., Williams, D.A., Simonelli, D.P., Breneman, H.H., Klaasen, K.P., Levanas, G., Denk, T., Galileo SSI Team, 2001. Imaging of volcanic activity on Jupiter's moon Io by Galileo during the Galileo Europa Mission and the Galileo Millennium Mission. J. Geophys. Res. 106, 33025–33052.

Kieffer, S.W., Lopes-Gautier, R., McEwen, A., Smythe, W., Keszthelyi, L., Carlson, R., 2000. Prometheus: Io's wandering plume. Science 288, 1204–1208.

Krueger, H., Horanyi, M., Krivov, A., Graps, A., 2002. Jovian dust: streams, clouds and rings. In: Bagenal, F., McKinnon, W., Dowling, T. (Eds.), Jupiter: Planet, Satellites and Magnetosphere. Colorado Univ. Press, Boulder. In press.

Lee, S.W., Thomas, P.C., 1980. Near-surface flow of volcanic gases on Io. Icarus 44, 280–290.

Lopes, R.M.C., Kamp, L.W., Doute, S., Smythe, W.D., Carlson, R.W., McEwen, S.A., Geissler, P.E., Kieffer, S.W., Leader, F.E., Davies, A.G., Barbinis, E., Mehlman, R., Segura, M., Shirley, J., Soderblom, L.A., 2001. Io in the near-infrared: Near-Infrared Mapping Spectrometer (NIMS) results from the Galileo flybys in 1999 and 2000. J. Geophys. Res. 106, 33053–33078.

Lopes, R.M.C., Kamp, L.W., Smythe, W.D., Mouginis-Mark, P., Kargel, J., Radebaugh, J., Turtle, E.P., Perry, J., Williams, D.A., Carlson, R.W., Douté, S., 2004. Lava lakes on Io: observations of Io's volcanic activity from Galileo NIMS during the 2001 flybys. Icarus. In press.

Lopes-Gautier, R., Davies, A.G., Carlson, R., Smythe, W., Kamp, L., Soderblom, L., Leader, F.E., Mehlman, R., 1997. Hot spots on Io: initial results from Galileo's near infrared mapping spectrometer. Geophys. Res. Lett. 24, 2439–2443.

Lopes-Gautier, R., McEwen, A.S., Smythe, W.B., Geissler, P.E., Kamp, L., Davies, A.G., Spencer, J.R., Keszthelyi, L., Carlson, R., Leader, F.E., Mehlman, R., Soderblom, L., The Galileo NIMS And SSI Teams, 1999. Active volcanism on Io: global distribution and variations in activity. Icarus 140, 243–264.

Lopes-Gautier, R., Doute, S., Smythe, W.D., Kamp, L.W., Carlson, R.W., Davies, G.A., Leader, F.E., McEwen, A.S., Geissler, P.E., Kieffer, S.W., Keszthelyi, L., Barbinis, E., Mehlman, R., Segura, M., Shirley, J., Soderblom, L.A., 2000. A close-up look at Io from Galileo's Near-Infrared Mapping Spectrometer. Science 288, 1201–1204.

Marchis, F., de Pater, I., Davies, A.G., Roe, H.G., Fusco, T., Le Mignant, D., Descamps, P., Macintosh, B.A., Prangé, R., 2002. High-resolution Keck Adaptive Optics Imaging of violent volcanic activity on Io. Icarus 160, 124–131.

McEwen, A.S., 1988. Global color and albedo variations on Io. Icarus 73, 385–426.

McEwen, A.S., Soderblom, L.A., 1983. Two classes of volcanic plumes on Io. Icarus 55, 191–217.

McEwen, A.S., Keszthelyi, L., Geissler, P., Simonelli, D.P., Carr, M.H., Johnson, T.V., Klaasen, K.P., Breneman, H.H., Jones, T.J., Kaufman, J.M., Magee, K.P., Senske, D.A., Belton, M.J.S., Schubert, G., 1998a. Active volcanism on Io as seen by Galileo SSI. Icarus 135, 181–219.

McEwen, A.S., Keszthelyi, L., Spencer, J.R., Schubert, G., Matson, D.L., Lopes-Gautier, R., Klaasen, K.P., Johnson, T.V., Head, J.W., Geissler, P., Fagents, S., Davies, A.G., Carr, M.H., Breneman, H.H., Belton, M.J.S., 1998b. High-temperature silicate volcanism on Jupiter's moon Io. Science 281, 87–90.

McEwen, A.S., Belton, M.J.S., Breneman, H.H., Fagents, S.A., Geissler, P., Greeley, R., Head, J.W., Hoppa, G., Jaeger, W.L., Johnson, T.V., Keszthelyi, L., Klaasen, K.P., Lopes-Gautier, R., Magee, K.P., Milazzo, M.P., Moore, J.M., Pappalardo, R.T., Phillips, C.B., Radebaugh, J., Schubert, G., Schuster, P., Simonelli, D.P., Sullivan, R., Thomas, P.C., Turtle, E.P., Williams, D.A., 2000. Galileo at Io: results from high-resolution imaging. Science 288, 1193–1198.

Milazzo, M.P., Keszthelyi, L.P., McEwen, A.S., 2001. Observations and initial modeling of lava–SO_2 interactions at Prometheus, Io. J. Geophys. Res. 106, 33121–33128.

Moore, J.M., Sullivan, R.J., Chuang, F.C., Head, J.W., McEwen, A.S., Milazzo, P.M., Nixon, B.E., Pappalardo, R.T., Schenk, P.M., Turtle, E.P., 2001. Landform degradation and slope processes on Io: the Galileo view. J. Geophys. Res. 106, 33223–33240.

Pearl, J.C., Sinton, W.M., 1982. Hot spots of Io. In: Morrison, D. (Ed.), Satellites of Jupiter. Univ. of Arizona Press, Tucson, pp. 724–755.

Perry, J., Radebaugh, J., Lopes, R., McEwen, A., Keszthelyi, L., 2003. Gish Bar Patera, Io: geology and volcanic activity, 1996–2001. In: Proc. Lunar Planet. Conf., p. 1720. Abstracts 34.

Phillips, C.B., 2000. Voyager and Galileo SSI views of volcanic resurfacing on Io and the search for geologic activity on Europa. PhD thesis, University of Arizona, Tucson.

Pieri, D.C., Nelson, R.M., Baloga, S.M., Sagan, C., 1984. Sulfur flows of Ra Patera, Io. Icarus 60, 685–700.

Porco, C., West, R., McEwen, A., Del Genio, A., Ingersoll, A., Thomas, P., Squyres, S., Dones, L., Murray, C., Johnson, T., Burns, J., Brahic, A., Neukum, G., Veverka, J., Barbara, J., Denk, T., Evans, M., Ferrier, J., Geissler, P., Helfenstein, P., Roatsch, T., Throop, H., Tiscareno, M., Vasavada, A., 2003. Cassini Imaging Science at Jupiter. Science 299, 1541–1547.

Radebaugh, J., Keszthelyi, L.P., McEwen, A.S., Turtle, E.P., Jaeger, W., Milazzo, M., 2001. Paterae on Io: a new type of volcanic caldera? J. Geophys. Res. 106, 33005–33020.

Radebaugh, J., McEwen, A.S., Milazzo, M., Keszthelyi, L.P., Davies, A., Turtle, E.P., Dawson, D., 2004. Observations and temperatures of Io's

Pele Patera from Cassini and Galileo spacecraft images. Icarus 169, 65–79.

Rathbun, J.A., Spencer, J.R., Tamppari, L.K., Martin, T.Z., Barnard, L., Travis, L.D., 2003. Mapping of Io's thermal radiation by the Galileo photopolarimeter-radiometer (PPR) instrument. Icarus. Submitted for publication.

Russell, C.T., Kivelson, M.G., 2001. Evidence for sulfur dioxide, sulfur monoxide, and hydrogen sulfide in the Io exosphere. J. Geophys. Res. 106, 33267–33272.

Sartoretti, P., McGrath, M.A., McEwen, A.S., Spencer, J.R., 1995. Post-Voyager brightness variations on Io. J. Geophys. Res. 100, 7523–7530.

Schenk, P., Hargitai, H., Wilson, R., McEwen, A., Thomas, P., 2001. The mountains of Io: global and geological perspectives from Voyager and Galileo. J. Geophys. Res. 106, 33201–33222.

Spencer, J.R., Shure, M.A., Ressler, M.E., Sinton, W.M., Goguen, J.D., 1990. Discovery of hotspots on Io using disk-resolved infrared imaging. Nature 348, 618–621.

Spencer, J.R., Schneider, N.M., 1996. Io on the Eve of the Galileo Mission. Ann. Rev. Earth Pl. Sci. 24, 125–190.

Spencer, J.R., Stansberry, J.A., Dumas, C., Vakil, D., Pregler, R., Hicks, M., Hege, K., 1997a. History of high-temperature Io volcanism: February 1995 to May 1997. Geophys. Res. Lett. 24, 2451–2455.

Spencer, J.R., McEwen, A.S., McGrath, M.A., Sartoretti, P., Nash, D.B., Noll, K.S., Gilmore, D., 1997b. Volcanic resurfacing of Io: post-repair HST imaging. Icarus 127, 221–237.

Spencer, J.R., McEwen, A.S., Sartoretti, P., Ballester, G.E., McGrath, M.A., Nash, D.B., 1997c. Hubble Space Telescope Observations of plumes and surface changes on Io. In: Io During the Galileo Era Conf., Lowell Observatory, Flagstaff, AZ, September 22nd–24th. Abstract.

Spencer, J.R., Sartoretti, P., Ballester, G.E., McEwen, A.S., Clarke, J.T., McGrath, M.A., 1997d. Pele plume (Io): observations with the Hubble Space Telescope. Geophys. Res. Lett. 24, 2471–2474.

Spencer, J.R., Jessup, K.L., McGrath, M.A., Ballester, G.E., Yelle, R., 2000. Discovery of Gaseous S2 in Io's Pele Plume. Science 288, 1208–1210.

Strom, R.G., Schneider, N.M., Terrile, R.J., Cook, A.F., Hansen, C., 1981. Volcanic eruptions on Io. J. Geophys. Res. 86, 8593–8620.

Strom, R.G., Schneider, N.M., 1982. Volcanic eruption plumes on Io. In: Morrison, D. (Ed.), Satellites of Jupiter. Univ. of Arizona Press, Tucson, pp. 598–633.

Turtle, E.P., Jaeger, W.L., Keszthelyi, L.P., McEwen, A.S., Milazzo, M., Moore, J., Phillips, C.B., Radebaugh, J., Simonelli, D., Chuang, F., Schuster, P., Galileo SSI Team, 2001. Mountains on Io: high-resolution Galileo observations, initial interpretations, and formation models. J. Geophys. Res. 106, 33175–33200.

Veeder, G.J., Matson, D.L., Johnson, T.V., Blaney, D.L., Goguen, J.D., 1994. Io's heat flow from infrared radiometry: 1983–1993. J. Geophys. Res. 99, 17095–17162.

Williams, D.A., Davies, A.G., Keszthelyi, L.P., Greeley, R., 2001. The summer 1997 eruption at Pillan Patera on Io: implications for ultrabasic lava flow emplacement. J. Geophys. Res. 106, 33105–33120.

Wilson, L., Head, J.W., 2001. Lava fountains from the 1999 Tvashtar Catena fissure eruption on Io: implications for dike emplacement mechanisms, eruption rates, and crustal structure. J. Geophys. Res. 106, 32997–33004.

Zhang, J., Goldstein, D.B., Varghese, P.L., Gimelshein, N.E., Levin, D.A., Gimelshein, S.F., 2002. Modeling low density sulfur dioxide volcanoes on Jupiter's moon Io. In: Proc. Lunar Planet. Sci. Conf., p. 1137. Abstract 33.